Theory of the martensitic transformation in cobalt

P. Tolédano,[1] G. Krexner,[2] M. Prem,[2,3] H.-P. Weber,[1] and V. P. Dmitriev[1]
[1]*Groupe "Structure Des Matériaux Sous Conditions Extrêmes," SNBL/ESRF BP220, 38043 Grenoble Cedex, France*
[2]*Institut für Experimentalphysik, Universität Wien, Bolzmanngasse 5, A-1090 Wien, Austria*
[3]*Laboratoire Leon Brillouin, CEA Saclay, F-91191 Gif sur Yvette, France*
(Received 14 March 2001; published 20 September 2001)

A phenomenological theory of the martensitic fcc-hcp transformation is proposed and applied to the illustrative example of cobalt. The fcc and hcp structures are shown to result from different ordering mechanisms from a disordered polytypic structure and to be intrinsically faulted. The three, fcc, hcp, and disordered polytype, structures are inserted in the framework of the segregation process which leads to the formation of close-packed structures from the melt. The essential features reported for the fcc-hcp transformation in cobalt are explained within the preceding model, namely, the asymmetry of the interphase region, the phonon spectrum, the δ-shape of its specific heat anomaly, and the existence of an intermediate modulated structure. The property of the transformation enthalpy to be different on heating and cooling is related to the different degree of order of the hcp and fcc structures. The partial dislocation mechanism currently assumed for the transformation is deduced from the secondary shear strains involved at the transformation.

DOI: 10.1103/PhysRevB.64.144104 PACS number(s): 64.70.Kb, 81.30.Kf

I. INTRODUCTION

Face centered cubic (fcc) and hexagonal close packed (hcp) structures coexist in the pressure-temperature phase diagrams of more than twenty elemental crystals,[1,2] but only for six of them (He, Fe, Co, Tl, Pb, and Yb) is there a direct transition between a fcc phase and the simplest (hcp) close-packed bilayer structure. Hence in the lanthanides Sm, Gd, Tb, Dy, and Y, the fcc and hcp phases are separated by higher-order polytypes, namely, the double hcp (dhcp) and nine-layered rhombohedral (9R) structures. In other lanthanides (La, Ce, Pr, Nd, Pm) and some heavy actinides (Am, Cm, Bk, Cf) the hcp phase is absent and only the fcc-dhcp and fcc-triple hcp (thcp) transitions take place. In Cs and Xe the high-pressure hcp and low-pressure fcc phases are separated by intermediate structures.

With the exception of cobalt all the elements displaying a fcc-hcp transition possess also a body centered (bcc) phase in their phase diagram. For example, in Fe, Tl and Yb the bcc phase occupies a large region of the phase diagram being adjacent to both the fcc and hcp phases. In these three elements the fcc and hcp structures can therefore be deduced from their parent bcc structure via the Bain deformation[3] and Burgers[4] mechanisms as described in Refs. 5 and 6. In contrast the phase diagram of cobalt, which has been recently explored up to 100 GPa and 3000 K (Ref. 7) shows no presence of a bcc phase. Accordingly the preceding mechanisms cannot be invoked for describing its fcc-hcp transformation. This remark holds for ^{3}He and ^{4}He for which the bcc phase occupies a restricted region of the corresponding phase diagrams[1] being exclusively in contact with the hcp phase, far from the region of stability of the fcc phase. In Pb the high-pressure bcc phase[8] seems also to have no contact with the fcc phase but the phase diagram is still largely unexplored.

The fcc-hcp transformation in Co is currently designated as martensitic[9–11] due to its diffusionless character, its considerable thermal hysteresis and the typical nucleation and growth processes. It shows a shape memory type effect which concerns the relative orientation of the fcc and hcp structures when cycling across the transition.[12] Furthermore the transformation temperature T_m, as well as the amount and extent of transformed structures is drastically affected by various factors, namely, the external stresses[13] or the alloying with soluble atoms (such as Fe and Ni)[14] or with metallic and nonmetallic elements of limited solubility range.[15] There exist however, a number of features which makes the transition in Co different than the martensitic transformations found, for example, in bcc-based metals and alloys. Thus the transformation, which takes place at $T_m \simeq 695$ K at ambient pressure is weakly first order, as attested by small changes in enthalpy ($\Delta h = 113$ cal mol^{-1} on heating) and volume ($\Delta V/V \simeq 3.3\times 10^{-3}$) and by a sharp singularity of the specific heat.[16] On the other hand no significant softening of the relevant phonon branches could be observed[17–21] in the low-temperature (hcp) or high-temperature (fcc) phases but only a slight decrease of the c_{44} hexagonal shear constant[19,21] when approaching T_m from the hcp phase. There is also a strong tendency to disordering of the structure which is reflected in the dependence with temperature of the width of some diffraction lines[22] and anomalous diffuse scattering[23] along certain directions in reciprocal space which can both be interpreted in terms of stacking faults.[24] In the region of coexistence of the two structures around T_m the disorder is also manifested in pure cobalt by the appearance of a modulated structure[23] and in cobalt alloys by the stabilization of high-order polytypes.[25,26]

Many theoretical models[10,27–39] have discussed the fcc-hcp transformation in metals and alloys. Most of them[27–35] focus on the transformation mechanism between the two close-packed structures described in terms of nucleation and growth processes. They differ in the details of the nucleation process and in the way the partial dislocations propagate from plane to plane. Other approaches are formulated in terms of shearing mechanisms,[4,10,36] or Fermi-surface mechanisms taking into account the average electron concen-

 ©2001 The American Physical Society

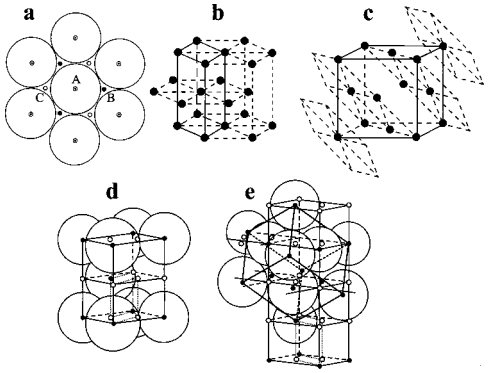

FIG. 1. (a) Close packing of hard spheres. Projection of the layers in the (001) plane. Centers of the circles are in *A* position, small solid dots represent the *B* position and small open circles denote the *C* position. (b) Two-layered hcp structure. (c) Three-layered fcc structure. (d) Unit-cell of the disordered polytype structure within the hcp structure. (e) Unit-cell of the disordered polytype structure within the fcc structure.

tration per atom.[37–39] None of the proposed models allow to give a comprehensive picture of the intricate variety of experimental features reported for the transformation in cobalt. The aim of the present work is to propose a unified description of this transformation in the framework of the segregation process which leads to the formation of the fcc and hcp close-packed structures from the melt. The observed properties of Co will be deduced from the ordering nature of the segregation mechanism and from the corresponding symmetry of the transformation order-parameter defined in terms of the proper critical variables and thermodynamic functions.

The article is organized as follows. In Sec. II we give a phenomenological description of the crystallographic and thermodynamic properties which characterize the fcc-hcp transformation extending the ideas developed in Ref. 40 and insert this description in a theoretical approach to the segregation of close-packed structures from the melt. We then illustrate the preceding model in the case of cobalt (Sec. III). In Sec. IV we summarize our results and conclude by underlining the properties which differentiate ordering-type martensitic transformations.

II. PHENOMENOLOGICAL THEORY OF THE FCC-HCP TRANSFORMATION

A. Crystallographic description and order-parameter symmetries

Although a close packing of atoms represented by hard spheres may be realized in several ways,[41,42] in real crystals close packing always corresponds to a layered configuration which gives the possibility of isolating planes of atoms packing in closest manner. These planes are stacked according to some rules of filling up space and they represent hexagonal packing of spheres each of which is in contact with six nearest neighbors [point *A* in Fig. 1(a)]. In the centers of the triangles formed by neighboring atoms exist geometrically equivalent sites denoted *B* and *C* in Fig. 1(a). A spatial close packing is realized when each of the successive layers occupy the free spacings left by the preceding layer related to positions of the *B* or *C* type. The stacking order of the layers determines the type of close packed structure. For the equiradii (*R*) close packed spheres shown in Fig. 1(a) in addition to the condition $a_h=b_h=2R$ where a_h and b_h are the hexagonal lattice parameters one has additional conditions reflecting the close packing in the third dimension: $c_h=a_h\sqrt{8/3}$ for a two-layer stacking structure, $c_h=a_h\sqrt{6}$ for a three-layer structure, etc.

The two-layered (hcp) and three-layered (fcc) structures represent the simplest close-packed configurations of hard sphere atoms. In their unit cells shown in Figs. 1(b) and 1(c) each layer is shifted with respect to the adjacent layer by $a_h\sqrt{3}$ in the $[120]_{\rm hcp}$ crystallographic direction. The basic vectors of the hcp unit cell is expressed in functions of the basic vectors of the fcc rhombohedral (primitive) unit cell as

$$\mathbf{a}_h=\mathbf{b}_c-\mathbf{c}_c,\mathbf{b}_h=\mathbf{a}_c-\mathbf{c}_c,\quad \mathbf{c}_h=\frac{2}{3}(\mathbf{a}_c+\mathbf{b}_c+\mathbf{c}_c). \tag{1}$$

From Eq. (1) or directly from the hcp and fcc structures, one can deduce that the maximal substructure common to the hcp and fcc structures is composed by a monolayer hexagonal structure which has the simple hexagonal symmetry D^1_{6h} and unit cell volume $V=V_h/6=V_c/3$ where V_h and V_c are the respective volumes of the hcp and fcc unit cells. Figures 1(d) and 1(e) show the unit cell of the substructure which we denominate the *L* structure within the hcp and fcc structures. One can see from these figures that the *L* unit cell is filled by 1/3 atoms, i.e., it corresponds to an occupancy $Z=1/3$ for the *L* structure. This fractional number must be understood as follows: In a given monolayer the atoms occupy the crystallographic position 1(a): (000) and only one among the three positions *A*, *B*, and *C* is occupied. In the next layer the atoms cannot be again in position *A* but only in position *B* or *C*, say *B*. In the following layer they will occupy the position *A* or *C*, and so forth. In other words the *L*-layer stacking corresponds to a statistically disordered polytype structure in which the *A*, *B*, and *C* sites are equivalent, the 1(a) positions being occupied with equal probabilities 1/3 by atoms. We will now assume that the polytype *L* structure is the *parent-structure* for our description of the fcc-hcp transition. With that goal let us write the basis vectors of the hcp and fcc unit cells in terms of the basis vectors $(\mathbf{a}_L,\mathbf{b}_L,\mathbf{c}_L)$ of the *L* structure:

$$\mathbf{a}_h=2\mathbf{a}_L-\mathbf{b}_L,\mathbf{b}_h=\mathbf{a}_L+2\mathbf{b}_L,\quad \mathbf{c}_h=2\mathbf{c}_L, \tag{2}$$

$$\mathbf{a}_c=\mathbf{a}_L+\mathbf{b}_L+\mathbf{c}_L,\mathbf{b}_c=-\mathbf{a}_L+\mathbf{c}_L,\quad \mathbf{c}_c=-\mathbf{b}_L+\mathbf{c}_L. \tag{3}$$

From Eqs. (2) and (3) one can deduce the wave vectors expressing the breaking of the translational symmetry at the virtual $L\rightarrow$hcp and $L\rightarrow$fcc transitions. One finds, respectively, $\mathbf{k}_{15}=\frac{1}{3}(\mathbf{a}^*_L+\mathbf{b}^*_L)+\frac{1}{2}\mathbf{c}^*_L$ and $\mathbf{k}_{10}=\frac{1}{3}(\mathbf{a}^*_L+\mathbf{b}^*_L+\mathbf{c}^*_L)$, where $\mathbf{a}^*_L$, $\mathbf{b}^*_L$, and $\mathbf{c}^*_L$ are the reciprocal lattice vectors of the *L*-hexagonal Brillouin zone. The notation of the $\mathbf{k}$ vectors refers to Kovalev's tables.[43]

(a) *The L-hcp transition.* The wave vector $\mathbf{k}_{15}$ associated with the *L*-hcp transition coincides with the *H* point of the

hexagonal Brillouin zone boundary.[44] Its invariance group is $\hat{G}(\mathbf{k}_{15})=D_{3h}$. Hence the star $\mathbf{k}_{15}^{\star}$ has two branches $\mathbf{k}_{15}^{1}=-\mathbf{k}_{15}^{2}=(4\pi/3a_L,0,\pi/c_L)$. Since the small irreducible representation IR $\hat{\tau}_1$ of D_{3h} which describes the permutation of atoms in the L structure is the identity IR, one can deduce the 2×2 matrices given in the Appendix, which generate the IR $\tau_1(\mathbf{k}_{15}^{\star})$ of the D_{6h}^{1} space group. Using the transformation properties of the matrices forming $\tau_1(\mathbf{k}_{15}^{\star})$ within a standard Landau procedure[45] one obtains the possible symmetries of the phases induced by $\tau_1(\mathbf{k}_{15}^{\star})$ and the equilibrium values of the corresponding two-component order parameter denoted $(\eta_1\,\eta_2)$. Three different symmetries are found: (i) $D_{6h}^{1}(V\times6)$ for $\eta_1=-\eta_2\neq0$, (ii) $D_{6h}^{4}(V\times6)$ for $\eta_1=-\eta_2\neq0$, and (iii) $D_{3h}^{1}(V\times6)$ for $\eta_1\neq\eta_2\neq0$. The second solution coincides with the sixfold unit cell and space group of the hcp structure. Accordingly the L-hcp transition corresponds to the equilibrium values of the two-component order parameter

$$\eta_1=-\eta_2=\eta\neq0. \tag{4}$$

At the crystallographic level the *ordering* mechanism taking place at the L-hcp transition corresponds to the splitting of the initial onefold site 1(a) into three twofold positions: 2(b): $(000,00\frac{1}{2})$, 2(c): $\pm(\frac{1}{3}\frac{2}{3}\frac{1}{4})$, and 2(d): $\pm(\frac{1}{3}\frac{2}{3}\frac{3}{4})$. Since in the initial disordered L-structure only one 1(a) position among three is occupied in the ordered hcp structure only one of the twofold positions will be occupied by two atoms. Actually as a result of close packing the hard sphere system of atoms will occupy either position 2(c) or 2(d) since they are crystallographically equivalent. The resulting two-layered hcp structure will fulfil the standard ratio for the unit cell parameters $c_h/a_h=\sqrt{8/3}\simeq1.63$.

(b)*The L-fcc transition.* The wave vector $\mathbf{k}_{10}$ associated with the L-fcc transition is located on the edge (the KH-line) of the hexagonal L-Brillouin zone.[44] Its invariance group is $\hat{G}(\mathbf{k}_{10})=C_{3v}$.[43] Therefore the star $\mathbf{k}_{10}^{\star}$ has four branches, which are $\mathbf{k}_{10}^{1}=-\mathbf{k}_{10}^{2}=(4\pi/3a_L,0,2\pi/3c_L)$ $\mathbf{k}_{10}^{3}=-\mathbf{k}_{10}^{4}=(4\pi/3a_L,0,-2\pi/3c_L)$. From the identity IR of C_{3v} one can construct the 4×4 matrices generating the IR $\tau_1(\mathbf{k}_{10}^{\star})$ which are given in the Appendix from which the possible symmetries induced by $\tau_1(\mathbf{k}_{10}^{\star})$ and the equilibrium values of the corresponding four-component order parameter denoted $(\zeta_1,\zeta_2,\zeta_3,\zeta_4)$ are obtained. One finds seven different symmetries: (i) $D_{6h}^{1}(V\times9)$ for $\zeta_1=\zeta_2=\zeta_3=\zeta_4$, (ii) $C_{3v}^{1}(V\times9)$ for $\zeta_1\neq\zeta_2\neq\zeta_3\neq\zeta_4$, (iii) $D_{3d}^{3}(V\times9)$ for $\zeta_1=\zeta_2,\zeta_3=\varepsilon^{*}\zeta_4$, (iv) $D_{3d}^{5}(V\times3)$ for $\zeta_1=\zeta_2\neq0,\zeta_3=\zeta_4=0$, (v) $C_{3v}^{5}(V\times3)$ for $\zeta_1=\zeta_2=0,\zeta_3\neq\zeta_4$, (vi) $D_{3h}^{1}(V\times9)$ for $\zeta_1=\zeta_3$ and $\zeta_2=\zeta_4$, and (vii) $C_{6v}^{1}(V\times9)$ for $\zeta_1\neq0,\zeta_2=\zeta_3=\varepsilon^{*}\zeta_4$. Only two of the preceding solutions (iv and v) involve a threefold multiplication of the L unit cell in agreement with Eq. (3). The solution iv actually coincides with the fcc symmetry $(O_h^5,Z=1)$ due to the specific crystallogeometrical conditions fulfilled by the L unit cell which are (i) a 1/3 occupancy of the L structure by the atoms and (ii) a ratio $c_L/a_L=\sqrt{2}$ corresponding to a close-packed structure. In order to understand why the fulfillment of the preceding conditions leads to a coincidence of the rhombohedral D_{3d}^{5} and cubic O_h^5 space groups let us clarify the crystallographic aspect of the $D_{6h}^{1}(L)\rightarrow D_{3d}^{5}(V\times3)$ ordering mechanism. In this mechanism the initial 1(a) position splits into 1(a) and 2(c): $\pm(\frac{1}{3}\frac{1}{3}\frac{1}{3})$ positions. Since atoms occupy only one of the 1(a) positions in the rhombohedral structure they are localized at lattice nodes but not on sites located inside the unit cells. This is illustrated in Figs. 2(a) and 2(b) showing that within the preceding unit cell the position denoted X, for example, is empty. Consequently additional fourfold rotations are created in the structure which are connected with the sixfold rotations of the L structure by $\{C_6^z|00c_L\}$ acting as $\{C_4^z|00c_L\}$. This correspondence is indicated in Fig. 2(a) in which the effect of a fourfold rotation transforms the position X into the position Y which is empty. The coincidence $D_{3d}^{5}\leftrightarrow O_h^5$ requires also that the close-packing condition $c_L/a_L=\sqrt{2}$ which is equivalent to a 60° angle between the basis vectors $\mathbf{a}_c$, $\mathbf{b}_c$, and $\mathbf{c}_c$ of the fcc rhombohedron should be satisfied. It is notorious that a rhombohedral structure possessing equal angles α between its basis vectors has the fcc cubic symmetry for $\alpha=60°$. Note in this respect that the $O_h^5\rightarrow D_{3d}^{5}$ lowering of symmetry corresponds to a ferroelastic transition[45] involving the spontaneous shear strain $e_4=e_{yz}$. Therefore the reverse mechanism $D_{3d}^{5}\rightarrow O_h^5$ assumed in our description of the $L\rightarrow$fcc transition requires to take into account e_4 as a secondary order parameter coupled to the pri-

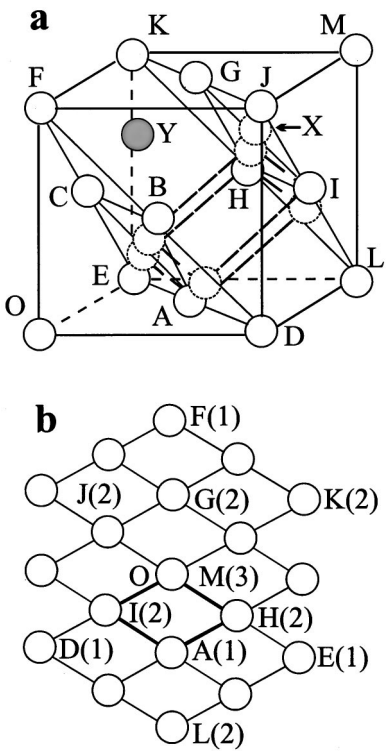

FIG. 2. Connection existing between the degree of occupancy of the latent phase and the $D_{3d}^{5}\rightarrow O_h^5$ increase in symmetry. In (a) a fourfold rotation exists only if atoms of the X type are absent. The Y position corresponds to the transformation of the X position under the effect of a fourfold rotation. (b) Projection on the (111) cubic plane of the fcc structure.

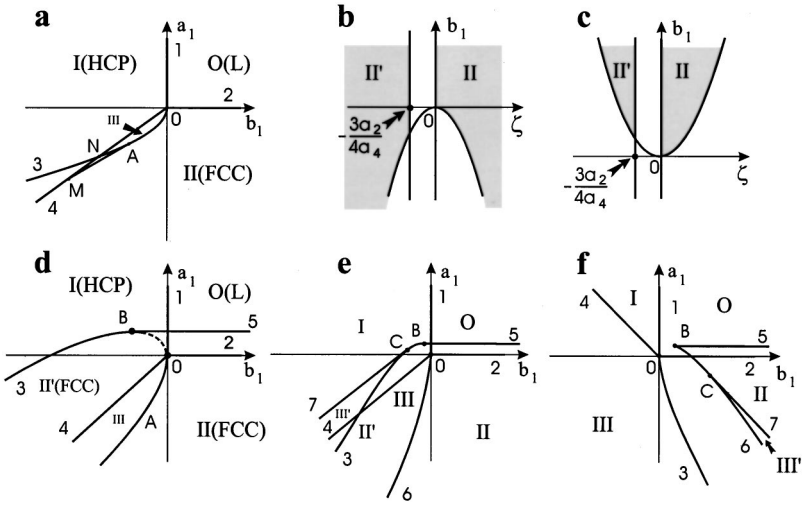

FIG. 3. Phase diagram corresponding to the order-parameter expansion expressed by Eq. (6): (a) when $\Delta=4a_3b_2-c^2<0$ and $c>0$ with $\varsigma>0$. (b) and (c) Existence of two disjuncted regions of stability for the fcc phase denoted II and II′, which are separated by a forbidden interval. (b) $c>0$, (c) $c<0$. (d) Phase diagram for $\Delta<0$ and $c>0$ but with two distinct regions of stability for the fcc phase. (e) and (f) Phase diagrams for $\Delta>0$ and (e) $c>0$ or (f) $c<0$. Phase III splits in this case into separated regions of stability (III and III′). In all the phase diagrams only the limit of stability lines are represented.

mary (ζ_i) order parameter in order to adjust the D_{3d}^5 rhombohedron to its close-packed O_h^5 form. Accordingly the L-fcc transition is associated with the nonvanishing components of the four-component order parameter:

$$\zeta_1=\zeta_2=\zeta\neq 0 \tag{5}$$

and to an eventual shear strain (e_4) acting as an adjusting secondary order parameter. In summary the fcc-hcp transformation can be interpreted as a transition between two ordered phases corresponding to different ordering mechanisms starting from a common disordered polytypic phase of hexagonal symmetry D_{6h}^1. In this interpretation the parent polytypic phase has been considered as a virtual structure which is not necessarily stabilized in the system. Its physical realization will be discussed in a more precise way in Sec. II C.

B. Phase diagrams

Let us work out the different types of phase diagrams involving the fcc and hcp phases which can be deduced from the preceding considerations. The transformation properties of the (η_i) $(i=1,2)$ and (ζ_i) $(i=1-4)$ order parameters respectively associated with the $L-$hcp and $L-$fcc transitions allow one to construct[45] the following independent invariants: $I_1=\eta_1^2+\eta_2^2$, $I_1'=\Sigma_{i=1}^4\zeta_i^2$, $I_2'=\zeta_1^3+\zeta_3^3-3(\zeta_1\zeta_2^2+\zeta_3\zeta_4^2)$, $I_3'=\Sigma_{i=1}^4\zeta_i^4$ where only monomials of degree $\leqslant 4$ have been taken into account. Using the equilibrium relationships (4) and (5) between the order parameter components in the hcp and fcc phases the preceding invariants reduce to the effective forms: $I_1=\eta^2$, $I_1'=\zeta^2$, $I_2'=\zeta^3$, $I_3'=\zeta^4$ which yield the effective order parameter expansion

$$F(T,P,\zeta,\eta)=F_0(T,P)+a_1\zeta^2+a_2\zeta^3+a_3\zeta^4+b_1\eta^2+b_2\eta^4+c\zeta^2\eta^2 \tag{6}$$

in which the lowest degree biquadratic coupling between ζ and η has been included. a_i, b_i, and c are phenomenological coefficients some of which may depend on temperature and pressure. The corresponding equations of state

$$\zeta(2a_1+3a_2\zeta+4a_3\zeta^2+2c\eta^2)=0, \tag{7}$$

$$\eta(2b_1+4b_2\eta^2+2c\zeta^2)=0 \tag{8}$$

have been discussed by Rochal.[46] They lead to different phase diagram topologies depending essentially on the signs of c, a_2, and $\Delta=4a_3b_2-c^2$. Figure 3(a) shows the phase diagrams corresponding to $c>0$ and $\Delta<0$ in the plane of the coefficients (a_1,b_1) which are assumed to vary linearly as functions of the two external variables T and P. It contains four phases denoted 0, I, II, and III. 0 is the L phase obtained for $\eta=0$, $\zeta=0$. I is the hcp phase forming for $\eta\neq 0$, $\zeta=0$. II is the fcc phase $(\eta=0,\zeta\neq 0)$. III is a *six-layered structure* which corresponds to the minimal superstructure common to the hcp and fcc structures. This additional stable state results from the coupling of the two irreducible order parameters (η_i) and (ζ_i) and is stabilized for $\eta\neq 0$ $\zeta\neq 0$. In Fig. 3(a) the boundaries (limit of stability lines) of the L phase with respect to the hcp and fcc phases are given by $b_1=0$ and $a_1=0$, respectively. The limit of stability of the hcp phase with respect to the fcc phase is also a straight line defined by the equation $a_1=cb_1/2b_2$ and the value of the hcp order parameter within phase I is given by $\eta^2=-b_1/2b_2$ with $b_1\leqslant 0$, $b_2>0$. The boundaries of the fcc phase II are determined by the equations

$$\zeta(3a_2+8a_3\zeta)\geqslant 0 \quad \text{and} \quad c\zeta+b_1\geqslant 0. \tag{9}$$

For positive values of ζ one has the situation found in Fig. 3(a) in which the boundaries of the fcc phase correspond to a parabolic branch and to the $a_1=0$ line. In this case the region of coexistence of the hcp and fcc phases contains the domain of stability of phase III. The topology of the phase diagram is more complicated if the value of the fcc order parameter ζ changes its sign. Figures. 3(b) and 3(c) (corresponding to $c>0$ and $c<0$, respectively) show that in this case there are two disjunct regions of stability for the fcc phase denoted II and II′, which are separated by a forbidden (unstable) interval for the ζ values $-(3a_2/4a_3)<\zeta<0$, where a_2 and a_3 are assumed to be positive (i.e., taking $a_2<0$ is equivalent to changing the sign of ζ in our considerations). Figure 3(d) shows the phase diagram corresponding

to the same conditions ($c>0, \Delta<0$), as in Fig. 3(a), but with two distinct regions of stability for the fcc phase denoted II and II′ which are separated by phase III. Note that phase II′ occupies a region of the ($a_1 b_1$) plane which is adjacent to phase II. Therefore a first-order anti-isostructural transition II-II′ corresponding to a change in the sign of ζ can occur. Figures. 3(e) and 3(f) represent the possible phase diagrams in which the conditions ($\Delta>0$, $c>0$) and ($\Delta>0$, $c<0$) hold, respectively. One can see that for such conditions phase III may also split into separated regions of stability determined by different signs of ζ. The effective coupled order parameter expansion given by Eq. (6) has the simplest form which can be taken for describing the phase diagrams associated with the (η_i) and (ζ_i) order parameters. More complex expansions can be assumed that would produce different topologies of the theoretical phase diagrams. Considering for example, a sixth degree term in η (i.e., a first-order L-hcp transition) may lead to a situation in which phase III becomes unstable and only a direct fcc-hcp transition takes place. Some of the qualitative features of the phase diagrams shown in Fig. 3 correspond, however, to specific properties of the fcc-hcp transition. In particular Fig. 3(a) shows that the region of coexistence of the two phases varies with decreasing values of a_1 and b_1, i.e., the discontinuous character of the transition changes with temperature and pressure and may reach as it is observed in some fcc-hcp transformations, a weakly first-order regime. A six-layered structure between the fcc and hcp structure and the antiisostructural phases (II′ and III′) are further remarkable features of the phase diagrams represented in Fig. 3.

C. Stacking faults and domain structure

From our proposed approach to the fcc-hcp transition one can deduce that the fcc and hcp structures are intrinsically faulted. There are two different origins for the stacking faults. One type of stacking fault which is symmetry induced and independent of temperature results form the existence of antiphase and orientational domains which occur at the L-hcp and L-fcc transitions. Another type of (temperature dependent) stacking fault relates to the ordering character of the order parameters. Let us first analyze the stacking faults associated with the domain texture of the phases. At the $L-$hcp transition the point group symmetry ($D^1_{6h} \rightarrow D^4_{6h}$) is not modified but one has a sixfold decrease of the translational symmetry expressed by Eq. (2). Therefore antiphase domains are created which transform into one another by the translations lost at the transition. Table I lists the equilibrium values of the two-component order parameter ($\eta_1 \eta_2$) for each of the six types of antiphase domains [column (b)] as well as the possible sequences of layers corresponding to each type of domain [column(c)]. For example, the first domain ($\eta - \eta$) implies a layer sequence of the type $\cdots CBCB \cdots$ whereas the domain ($-\eta\eta$) yields the sequence $\cdots BCBC \cdots$. The symmetry operators which transform the antiphase domain denoted 1 into the other antiphase domains are listed in column (d). The domain texture in the hcp phase must be compatible with the atomic packing. This excludes certain contacts between the domains that would generate sequences

TABLE I. Antiphase domains corresponding to the L-hcp transition. (b) Equilibrium values of the two-component order-parameter (η_1, η_2) for each of the six types of antiphase domains numbered in column (a). (c) Sequence of layers corresponding to each type of domain. (d) Symmetry operations transforming the domain 1 into the other domains. $\omega = \exp\{i\pi/3\}, \varepsilon = \exp\{2i\pi/3\}$.

(a)	(b)	(c)	(d)
1	$\eta\ -\eta$	$CBCB$	$\{C_1\|000\}$
2	$-\eta\ \eta$	$BCBC$	$\{C_1\|c_L\}$
3	$\varepsilon\eta\ \ \omega\eta$	$ABAB$	$\{C_1\|a_L\}$
4	$\omega^*\eta\ \varepsilon^*\eta$	$BABA$	$\{C_1\|a_L+c_L\}$
5	$\varepsilon^*\eta\ \omega^*\eta$	$ACAC$	$\{C_1\|-a_L\}$
6	$\omega\eta\ \varepsilon\eta$	$CACA$	$\{C_1\|\ -a_L+c_L\}$

of the type AA, BB, or CC. Therefore, the number of allowed contacts is limited. Using the standard notation[47] which labels h a hexagonal layer having an identical surrounding (e.g., B in ABA) and c a hexagonal layer having a nonsymmetrical surrounding (e.g., B in ABC) one finds two sorts of possible contacts $\cdots hhhchhh \cdots$ and $\cdots hhhcchhh \cdots$ which both correspond to *deformation* stacking faults.[47]

At the L-fcc transition the underlying change in the point-group symmetry ($D_{6h} \rightarrow D_{3d}$) and the corresponding threefold multiplication of the L unit cell lead to two different types of domains: (i) *two* orientational domains transforming into one another by the lost sixfold rotation and (ii) *three* antiphase domains. Table II lists the six different types of domains and the corresponding equilibrium values of the four-component order-parameter (ζ_i). In column (c) of Table II one finds the layer sequences associated with each domain e.g., $\cdots ACBACB \cdots$ for ($\zeta, \zeta, 0, 0$) and $\cdots BACBAC \cdots$ for ($\varepsilon, \zeta, \varepsilon^*, \zeta 0, 0$). Column (d) indicates the symmetry operators which transform the first domain into the others.

As for the L-hcp transition the contacts between the domains in the fcc structure must preserve the atomic close packing. At variance with the hcp structure one finds two types of stacking faults: (1) deformation-type stacking faults resulting from the contact between for example, the domains denoted 1 and 3 in Table II. It gives the layer stacking

TABLE II. Antiphase and orientational domains corresponding to the L-fcc transition. (a) Numbering of the domains. (b) Equilibrium values of the four-component order parameter ($\varsigma_1, \varsigma_2, \varsigma_3, \varsigma_4$) for each domain. (c) Layer sequences associated with each domain. (d) Symmetry operations transforming the first domain into the others. $\varepsilon = \exp\{2i\pi/3\}$.

(a)	(b)	(c)	(d)
1	$\varsigma\ \varsigma\ 0\ 0$	$ACBACB$	$\{C_1\|000\}$
2	$\varepsilon\varsigma\ \varepsilon^*\varsigma\ 0\ 0$	$BACBAC$	$\{C_1\|b_L\}$
3	$\varepsilon^*\varsigma\ \varepsilon\varsigma\ 0\ 0$	$CBACBA$	$\{C_1\|-a_L\}$
4	$0\ 0\ \varsigma\ \varsigma$	$ABCABC$	$\{\sigma_z\|000\}$
5	$0\ 0\ \varepsilon\varsigma\ \varepsilon^*\varsigma$	$CABCAB$	$\{\sigma_z\|a_L\}$
6	$0\ 0\ \varepsilon^*\varsigma\ \varepsilon\varsigma$	$BCABCA$	$\{\sigma_z\|2a_L\}$

$\cdots ACBABACB\cdots$ corresponding to $\cdots ccchhccc\cdots$ (2) Twining (growth) stacking faults due, for example, to the contacts between the domains denoted 1 and 4. The layer sequence is in this case $\cdots ACBABCABC\cdots$ corresponding to $\cdots ccchccc\cdots$.

Accordingly the domain structure and the structure of the domain walls lead to intrinsically faulted hcp and fcc structures the distribution of stacking faults being symmetry induced. These stacking faults are independent from temperature, i.e., they cannot be annihilated by external fields (aging, annealing, etc.) and give rise to a single domain, since we deal with a probabilistic mechanism with no conjugated field. Another type of temperature-dependent defects can be found in the close-packed fcc and hcp structures originating in the nonmaximal character of the order parameters which is inherent to the assumed ordering-type mechanism. In the disordered polytype structure each close-packed layer corresponds to a stacking fault. The ordering process leading to the hcp and fcc structures can be characterized by the number

$$\Delta = 1 - \frac{N_d}{N}, \tag{10}$$

where N is the total number of close packed layers and N_d is the number of stacking faults. N_d/N represents the concentration of stacking faults and one has $\Delta = 0$ in the disordered polytype structure and $\Delta = 1$ in the ideal close packed structures. Intermediate states correspond to $0 < \Delta < 1$. The value of Δ at a given temperature and pressure is determined by the number of defects. Far from the transition within the close packed phases, the asymptotic value of Δ will reflect the symmetry induced type of stacking faults. Close to the transition Δ accounts as well for the temperature dependent defects. In the following subsection we formalize such considerations in the framework of a phenomenological description of the ordering of close-packed structure which is inspired by a model of segregation in complex fluids.[48] This will give a more realistic picture of the parent polytype structure assumed in our approach.

III. SEGREGATION PROCESS TO CLOSE PACKED STRUCTURES

Let us consider the transformation from the melt to a structure formed by stacked hexagonal layers. The symmetry of the isotropic liquid is the extended Euclidean group $\tilde{E}_3 = O(3) \times R^3$ where $O(3)$ is the full orthogonal group and R^3 is the three-dimensional group of continuous translations. The IR's of $\tilde{E}_3$ are spanned by the basis functions[49]

$$\Phi^{\pm m}_{\mathbf{k}_j}(r,\theta,\varphi) = e^{i\mathbf{k}_j\cdot\mathbf{r}} \cdot Y^l_m(\theta,\varphi), \tag{11}$$

where the $\mathbf{k}_j$ are the infinite set of wave vectors ending on a sphere of given radius $|\mathbf{k}_j|$ and transforming into one another by the symmetry operators of $O(3)$. The Y^l_m ($m = -l, \ldots, +l$) are the spherical harmonics of order l. The infinite-dimensional IR's of $\tilde{E}_3$ are denoted D^{mk_j}. For given m two conjugated functions $\Phi^{\pm m}_{\mathbf{k}_j}$ are needed to construct a real (physically irreducible) representation.

Let $\rho_0(\mathbf{r}) = \text{const}$ be the probability density of atoms in the isotropic state and $\rho_s(\mathbf{r})$ the corresponding probability density in a segregated state. The increment $\delta\rho = \rho_s(\mathbf{r}) - \rho_0(\mathbf{r})$ can be expanded on the $\Phi^{\pm m}_{\mathbf{k}_j}$:

$$\delta\rho(\mathbf{r}) = \sum_{\mathbf{k}_j} \eta^{m\mathbf{k}_j} \cdot \Phi^{\pm m}_{\mathbf{k}_j}(r,\theta,\varphi). \tag{12}$$

The coefficients $\eta^{m,\mathbf{k}_j}$ define the components of the infinite-dimensional order-parameter associated with the transition between the isotropic liquid and a segregated state. Since the transition corresponds to an ordering mechanism the $\eta^{m,\mathbf{k}_j}$ necessarily transform as the IR denoted D^{0k_j}, i.e., they correspond to the set $\{\eta^{0\mathbf{k}_j}\}$ (denoted hereafter as $\{\eta_{\mathbf{k}_j}\}$). This results from the following arguments: Any IR of $\tilde{E}_3$ is constructed from a small IR (τ_1) associated with the invariance group of one branch (say $\mathbf{k}_1$) of the star $\mathbf{k}^\star_1$ which is $G_{\mathbf{k}_1} = SO(2)$.[50] Since the "unit cell" of the parent isotropic state is reduced to a single atom which is invariant under all the symmetry operations of $\tilde{E}_3$ τ_1 will necessarily coincide for an ordering mechanism,[51,52] with the *identity* IR of $SO(2)$ corresponding to $m = 0$. D^{0k_j} is spanned by the basis functions $\Phi^0_{\mathbf{k}_j} = Y^0_0 \cdot e^{i\mathbf{k}_j\cdot\mathbf{r}}$ where the arbitrarily oriented wave-vectors $\mathbf{k}_j$ belong to the same star. It follows immediately that the nth power invariants of the order-parameter components $I_n(\eta_{\mathbf{k}_j})$ correspond to products of the basis functions determined by the conditions $\Sigma^n_{i=1}\mathbf{k}_i = 0$. Therefore the variational free-energy density $F(\eta_{\mathbf{k}_j})$ associated with the transition from the isotropic state will contain invariants of all powers n except the linear invariant $I_1(\eta_{\mathbf{k}_j})$ which has been implicitly excluded from Eq. (12) by assuming a lowering of symmetry when going from the isotropic to the segregated state. In particular (one or two) cubic invariants will be present. Hence the transition to the segregated state is necessarily first order except essentially at an isolated point of the phase diagram (Landau point) where the coefficient of the (single) cubic invariant vanishes identically.

Depending on the number of nonvanishing independent $\mathbf{k}_j$ and on the respective equilibrium values of the $\eta_{\mathbf{k}_j}$ different segregated phases can be stabilized below the isotropic state whose symmetries correspond to subgroups of G of $\tilde{E}_3$. Figure 4 show the orientation of the wave vectors involved in the formation of the hcp and fcc structures from the melt. Hence the hcp structure requires three independent wave-vectors of equal lengths $|\mathbf{k}_j| = 3\sqrt{3}$ pertaining to a twelve arms irreducible star[43,45] with the following orientations in the hexagonal reciprocal space shown in Fig. 4. $\mathbf{k}_1 // [\bar{4},4,1]$, $\mathbf{k}_2 // [0,\bar{4},1]$, $\mathbf{k}_3 // [\bar{4},0,1]$, $\mathbf{k}_4 // [4,4,\bar{1}]$, $\mathbf{k}_5 // [0,\bar{4},\bar{1}]$, $\mathbf{k}_6 // [\bar{4},0,\bar{1}]$, and $\mathbf{k}_{i+6} = -\mathbf{k}_i$ ($i = 1-6$). The twelve components of the corresponding order-parameter fulfil the equilibrium relationships $\eta_{\mathbf{k}_i} = \eta_{\mathbf{k}}$ ($i = 1-12$) which gives rise to the effective free-energy density, associated with the isotropic-hcp transformation

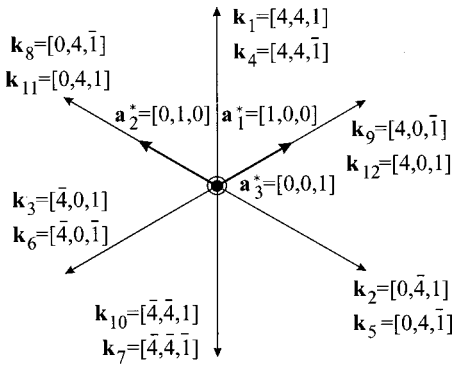

FIG. 4. Orientation of the wave-vectors involved in the formation of the hcp and fcc structures from the melt in projection on the (001) hexagonal reciprocal lattice plane.

$$F(\eta_{\mathbf{k}}) = a_1 \eta_{\mathbf{k}}^2 + a_2 \eta_{\mathbf{k}}^3 + a_3 \eta_{\mathbf{k}}^4 + \cdots . \tag{13}$$

The segregation of a fcc structure involves an eight-armed star whose branches are $\mathbf{k}_1$, $\mathbf{k}_2$, $\mathbf{k}_3$, $\mathbf{k}_6 // [\bar{4},\bar{4},\bar{1}]$, $\mathbf{k}_8 // [0,4,\bar{1}]$, $\mathbf{k}_9 = -\mathbf{k}_3$, $\mathbf{k}_{13} = [0,0,3]$, and $\mathbf{k}_{14} = -\mathbf{k}_{13}$. One has again for the eight components of the corresponding order-parameter: $\eta_{\mathbf{k}_i} = \eta_{\mathbf{k}}$ $(i = 1-8)$, i.e. the free-energy density associated with the formation of a fcc structure from the melt has the same effective form expressed by Eq. (13).

The ordering process which leads to the formation of hcp and fcc structures proceeds via the formation of lamellas (plates) of different thickness[53] with a progressive coalescence of the neighboring lamellas. One can therefore infer the existence below the melt of segregated regions in which the layers form short range sequences (e.g., hcp or fcc sequences) alternating with nonsegregated regions in which the layers are randomly stacked (disordered polytypes). Let us denote $\xi_{\mathbf{k}}$ the normalized probability for a given layer to be in a segregated region in the direction defined by the $\mathbf{k}$ vector and assume the order-parameter $\eta_{\mathbf{k}}$ to be a function of $\xi_{\mathbf{k}}$. The explicit form for $\eta_{\mathbf{k}}(\xi_{\mathbf{k}})$ for a given segregated structure, can be obtained by minimizing the thermodynamic potential

$$\int \{F[\eta_{\mathbf{k}}(\xi_{\mathbf{k}})] + g(\nabla \eta_{\mathbf{k}})^2\} d\xi_{\mathbf{k}}, \tag{14}$$

where the integral is over a volume in the $\xi_{\mathbf{k}}$ space. F is the free-energy density given by Eq. (13) and the Ginzburg g-invariant accounts for the fluctuations of $\eta_{\mathbf{k}}$ with respect to $\xi_{\mathbf{k}}$. One gets the equation of state

$$g \frac{d^2 \eta_{\mathbf{k}}}{d\xi_{\mathbf{k}}^2} = a_1 \eta_{\mathbf{k}} + \frac{3}{2} \eta_{\mathbf{k}}^2 + 2a_3 \eta_{\mathbf{k}}^3 + \cdots . \tag{15}$$

When the right-hand expansion is restricted to the third power Eq. (15) coincides with the general elliptic equation[54] which can be solved exactly[55]. More generally the bifurcation from the solution $\eta_{\mathbf{k}}(0) = 0$ which corresponds to the isotropic state, to the solution $\eta_{\mathbf{k}}(\xi_{\mathbf{k}}) \neq 0$ corresponding to a fully or partially segregated state can be obtained by linearizing Eq. (15) around the value $\eta_{\mathbf{k}}(0) = 0$.[56] One gets the second-order linear differential equation

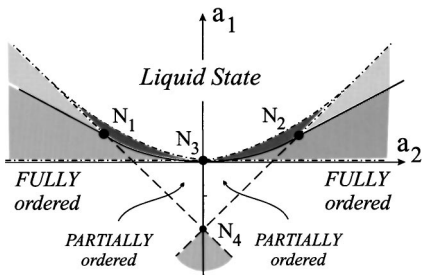

FIG. 5. Phase diagram corresponding to the equation of state (18) showing the topology of the partially and fully ordered close-packed states below the melt.

$$g \frac{d^2 \eta_{\mathbf{k}}^*}{d\xi_{\mathbf{k}}^2} = a_1^* \eta_{\mathbf{k}}^*, \tag{16}$$

where $\eta_{\mathbf{k}}^*$ is the eigenfunction corresponding to the eigenvalue a_1^* at which the solution $\eta_{\mathbf{k}}(\xi_{\mathbf{k}}) \neq 0$ branches off the solution $\eta_{\mathbf{k}}(0) = 0$. Taking into account the boundary conditions defining the initial isotropic state $[\eta_{\mathbf{k}}(0) = 0]$ and the fully segregated (ordered) state $[\eta_{\mathbf{k}}(1) = 1]$ one finds the asymptotically exact solution,[56] in the vicinity of $a_1 = a_1^*$ which is expressed as

$$\eta_{\mathbf{k}}(\xi_{\mathbf{k}}) = \eta_{\max}^{\mathbf{k}} \left| \sin \frac{\pi}{2} \xi_{\mathbf{k}} \right|, \tag{17}$$

where the amplitude $\eta_{\max}^{\mathbf{k}}$ is to be determined by the nonlinear terms in Eq. (15) and depends on the coefficients g, a_1, (a_1^*), a_2, $a_3, \ldots$. The periodic dependence expressed by Eq. (17) has two levels of interpretation in terms of the crystal structure. It shows on the one hand, that in the ordering process the crystal stratifies periodically forming successive stacked regions in which on the other hand, there is a sinusoidal-type variation from partially ordered to fully ordered subregions. Introducing the function $\eta_{\mathbf{k}}(\xi_{\mathbf{k}})$ given by Eq. (17) in the effective free-energy density $F(\eta_{\mathbf{k}})$ one gets by minimizing F with respect to ξ_k the equation of state

$$\eta_{\mathbf{k}} \frac{\partial \eta_{\mathbf{k}}}{\partial \xi_{\mathbf{k}}} (a_1 + 3\eta_{\mathbf{k}} + 4a_3 \eta_{\mathbf{k}}^2) = 0. \tag{18}$$

In addition to the isotropic (disordered) state ($\eta_{\mathbf{k}} = 0$ for $\xi_{\mathbf{k}} = 0$) one obtains the fully segregated (ordered) state for $\partial \eta_{\mathbf{k}} / \partial \xi_{\mathbf{k}} = 0$, i.e., for $|\cos(\pi/2)\xi_{\mathbf{k}}| = 0$ which yields $\xi_{\mathbf{k}} = 1$. The partially segregated state corresponds to the equilibrium values $\eta_{\mathbf{k}}$:

$$\eta_{\mathbf{k}}^e \simeq \sin \frac{\pi}{2} \xi_{\mathbf{k}}^e = -\frac{3a_2 \pm (9a_2^2 - 32a_1 a_3)^{1/2}}{8a_3}. \tag{19}$$

In contrast to the fully ordered state which coincides with a fixed limit value of $\xi_{\mathbf{k}}^e = 1$ the $\xi_{\mathbf{k}}^e$ values associated with partially ordered regions vary with the phenomenological coefficients of the free-energy density, i.e., they vary with temperature and pressure.

Figure 5 shows the phase diagram associated with the equation of state (18) assuming that a_3 is positive. Thus, the

partially and fully segregated (ordered) states which display an identical (e.g., hcp or fcc) symmetry are separated by lines of topological transformations which are determined by the property that the probability $\xi_{\mathbf{k}}$ reaches its maximal value $\xi_{\mathbf{k}}=1$. The two partially and fully ordered states bounding such lines can be reached from the isotropic state across first order transition lines and meet at a three-phase point denoted N_1 (or N_2) in Fig. 5. Note that close to the Landau point N_3 the isotropic to ordered state transformation is weakly first order. Note also that each segregated region possesses a symmetric analog corresponding to an opposite sign for $\eta_{\mathbf{k}}(\xi_{\mathbf{k}})$, i.e., each stable state has an anti-isostructural analog. The existence of antiisostructural states has been already noted in the phase diagrams of Figs. 3(b), 3(c), and 3(d).

From the preceding results one can infer a qualitative scheme for the segregation process leading to the formation of close-packed structures below the melt. In the partially ordered state shown in Fig. 5 the crystal is organized in a periodic array of stacked domains in which lamellas of ordered (hcp or fcc) structure are surrounded by disordered sequences of close packed polytypes. On cooling and approaching the fully ordered state the fraction of disordered sequences of layers reduce in each domain increasing the thickness of the lamellas, and simultaneously the neighboring domains tend to coalesce. At the topological transition the fusion of the domains is achieved and the phase is formed by an ordered close packed structure. This picture provides a justification and an interpretation of the disordered polytype structure which has been assumed from symmetry considerations (Sec. IIA) to be the parent structure for the fcc and hcp structures. Let us stress that for a realistic description of the close packed structures the picture has to be completed by taking into account the existence of stacking faults as discussed in Sec. II C.

Consequently the fcc-hcp transformation will be favored if the system is in the partially ordered state since the coherency stresses between the two structures will be reduced. In contrast the transformation will take place more abruptly when approaching the fully ordered state. This is attested by the form of the region of coexistence between the fcc and hcp structures found for example in La,[57] Pr,[58] and Nd[59] which merges at high temperature and enlarges at low temperature, going from weakly first-order to a strongly first-order regime. To our knowledge the fcc-hcp transformation in ^{4}He is the only counterexample to such a behavior, i.e., the region of coexistence between the two phases becomes more narrow on cooling from about 30 to 14 K as found by Frank and Daniels.[60,61] However, this exception can be explained by the Nernst principle as assumed by these authors.

IV. THE MARTENSITIC TRANSFORMATION IN COBALT

In this section we show that the fcc-hcp martensitic transformation in cobalt provides a concrete illustrative example of the general considerations developed in Sec. II. The essential experimental features of the transformation are interpreted in terms of its reordering and reconstructive characters.

A. Specific features of the transformation in Co

The hcp(α or ε)$\rightarrow$fcc(β or γ) transformation in Co takes place around $T_m=695$ K at ambient pressure more than one thousand degree below the melting transition ($T_f=1768$ K).[1,2] With increasing pressure up to above 70 GPa, the hcp-fcc transition line remains almost parallel to the melting line.[7] The fact that the fcc structure is always stable above the hcp structure has been attributed to the presence of magnetism which favors the hcp phase as a ground state.[62,63] Despite the loss of group-subgroup relationship between the symmetries of the phases which typifies reconstructive phase transitions[64] the transition in Co has a weakly discontinuous (first-order) character. This is attested by the small jump in enthalpy ($\Delta h\sim 113$ cal mol^{-1} on heating[65]) and volume ($\Delta V/V=0.329\%$)[16] involved at T_m and by a relatively small hysteresis of about 20 K at ambient pressure.[65] It is also reflected in the close relationship between the structural features of the two phases,[10,66] namely, (1) the distance between the close packed planes varies only by about 0.3% at T_m both structures displaying the almost ideal close packed rate $c/a\simeq 1.623$, (2) the same atomic coordination exists for the first and second nearest neighbors, and (3) the fcc and hcp lattices reversibly connect with the epitaxial relationships $(111)_{\mathrm{fcc}}//(001)_{\mathrm{hcp}}$ and $[11\bar{2}]_{\mathrm{fcc}}//[120]_{\mathrm{hcp}}$.

The main distinctive feature of the transformation in Co is the strong asymmetry of the fcc$\rightarrow$hcp and hcp$\rightarrow$fcc thermodynamic paths which manifests in the following properties: (i) The average value of the transformation enthalpy is different on heating (113 cal mol^{-1}) and cooling (84 cal mol^{-1}).[65] (ii) The hcp$\rightarrow$fcc transformation is always complete but the reverse fcc$\rightarrow$hcp transformation is incomplete: even at room temperature weak reflections of the fcc structure are still present. (iii) The dhcp ε' phase found at high pressure[7] is stabilized on quenching the fcc phase but not on heating the hcp phase. (iv) The disorder behavior of hcp and fcc Co differ greatly.[24] The fcc phase just above T_m is well ordered. In contrast a stacking disorder is always present in the hcp phase even during the early stages of the transformation. This is attested by the observation of diffuse streaks along the $[10\varsigma]$ hcp direction which are not detected in the fcc structure.[24] Analysis of the Debye-Waller factor reveals no anomaly in the hcp phase but an increase of the atomic square amplitude in the fcc phase on approaching T_m from above.[21](v) The fcc and hcp precursor regimes are also different.[24] In the hcp phase small but distinct preformed cubic lamellae with a volume ratio of 1/100 (fcc/hcp) exist far below T_m and start to grow at 20 K below T_m. Some ten degrees above T_m small hcp ordered packets exist which do not survive above the hysteresis region.[24] Independently from the cubic domains the c_{44} hexagonal elastic constant decreases some 50 K below T_m by above 27%,[19] but the corresponding fcc constant $[\frac{1}{3}(c_{11}-c_{12}+c_{44})]$ shows no equivalent.[21]

Other intriguing features of the transformation in Co are: (1) the form of the specific heat anomaly which shows a sharp increase from both sides of T_m with almost the same slope,[67] at variance with the current shape of c_p found at first-order transformations.[64] (2) The absence of soft mode

behavior[64] when approaching T_m from the fcc or hcp sides despite the c_{44} anomaly, which is accompanied by an increase of the internal friction[68] and a simultaneous decrease of the entire branch of transverse acoustic vibration corresponding to the mode. In the following subsections we give a unified description of the preceding properties in the framework of the theoretical model developed in Sec. II.

B. Asymmetry of the interphase region

The fcc-hcp transformation has been assumed in Sec. II A to take place between two differently ordered structures corresponding to the distinct set of effective order-parameter components: $(\eta,-\eta)$ for the hcp phase and $(\varsigma,\varsigma,0,0)$ for the fcc phase. As shown recently for reconstructive transformations between SiO_2 polymorphs[69] when two adjacent phases are associated to distinct subgroup symmetries of a parent phase their interphase is asymmetric. Furthermore, if one considers a thick phase boundary, i.e., not reduced to one or two layers, there exists a surface S_m inside the phase boundary which coincides with a minimal deformation. Therefore the volumes of the phases on each side of S_m will be different and possess the respective symmetries of the phases. On the other hand, since at the surface S_m one shifts from one to another set of order-parameter components $(\eta,-\eta)\rightarrow(\varsigma,\varsigma,0,0)$, the symmetry of the S_m surface will correspond to a cross section of the parent phase.

The preceding picture applies to the fcc-hcp transformation in Co. It is consistent with the difference of fcc and hcp volumes involved in the region of coexistence of the two phases which is much larger on the hcp side than on the fcc side. The S_m surface has in Co the simple hexagonal symmetry D_{6h}^1 of the disordered polytype structure and the phase boundary between the hcp and fcc interphase volumes should be macroscopically distorted by the shear strain e_{xy} required for the formation of the fcc close-packing but not for the hcp structure.

C. Specific heat anomaly

Since the transformation occurs between two differently ordered structures the order-parameter moduli corresponding to the hcp and fcc phases fulfill the conditions

$$\frac{\eta}{\eta_{\max}^{\mathbf{k}}}=\frac{\varsigma}{\varsigma_{\max}^{\mathbf{k}}}=1, \tag{20}$$

where $\mathbf{k}$ is the wave vector corresponding to the ΓA direction in the hexagonal Brillouin zone and to the ΓL direction in the cubic Brillouin zone. Therefore the temperature dependence of the effective order-parameter associated with the direct fcc-hcp mechanism will display a steplike behavior represented in Fig. 6(a). Such behavior is typical of reconstructive transitions between fully ordered phases.[64] From the conditions (20) one can deduce that the specific heat $c_p=-T(\partial^2F/\partial T^2)_p$ where F is given by Eq. (7) has the same expression on both sides of T_m: $c_p^{\mathrm{hcp}}=c_p^{\mathrm{fcc}}=-T(\partial^2F_0/\partial T^2)_p$. Therefore $(\Delta c_p)_{T=T_m}=0$, i.e., no jump of the specific heat takes place at the transition. This is in contrast with the upward jump found for Δc_p on cooling at first- and second-order transitions between group-subgroup related phases.[45] On the other hand, assuming $a_1=a_0(T-T_{c_1})$ and $b_1=b_0(T-T_{c_2})$ in Eq. (6) where a_0 and b_0 are positive constants one finds a finite discontinuity of the entropy $S=-\partial F/\partial T$ at T_m which on cooling is given by

$$S_{\mathrm{fcc}}-S_{\mathrm{h_{cp}}}=b_0(\eta_{\max}^{\mathbf{k}})^2-a_0(\varsigma_{\max}^{\mathbf{k}})^2. \tag{21}$$

Accordingly[70] $c_p(T)$ will display a narrow δ-shaped peak at T_m as shown in Fig. 6(b). The two preceding properties of the specific heat ($\Delta c_p=0$ and δ-shaped peak at T_m) have been shown[64] to constitute a typical signature of reconstructive transformations. Such properties are well illustrated by the experimental curve found for $c_p(T)$ in cobalt[67] which is reproduced in Fig. 6(c).

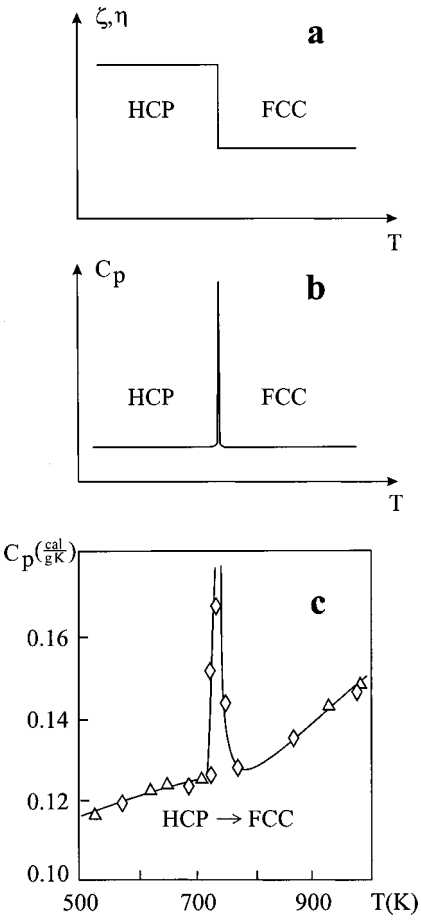

FIG. 6. Temperature dependence of (a) the order parameter and (b) the specific heat c_p across a transition between fully ordered hcp and fcc states. (c) Specific heat anomaly measured at the fcc-hcp transformation in cobalt from Ref. 67.

D. Degree of order in the fcc and hcp structures

The antiphase and orientational domains associated with a transition from a disordered polytype structure to hcp and fcc structures are listed in Tables I and II. It has been stressed (Sec. II C) in our description of the ordering process to close packed structures that the preceding transitions should occur

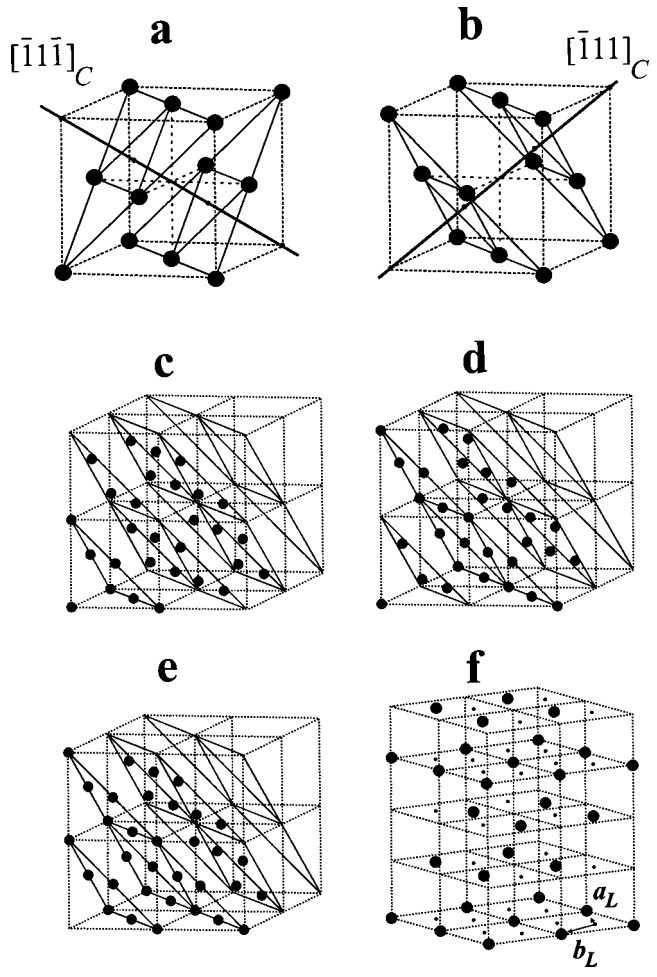

FIG. 7. (a) and (b): Two among the four cubic orientational domains within the hcp structure formed by $BCBCBC\cdots$ sequences of hexagonal close packed planes in the cubic framework and corresponding to the [0001] hexagonal direction. (c)–(e) Three antiphase domains in the hcp structure associated with one cubic domain and corresponding to $ABAB\cdots$ (c), $ACAC\cdots$ (d), and $CBCB\cdots$ (d) sequences. (f) One of the three type of antiphase domains formed at the hcp→fcc transformation and corresponding to the $ABCABC\cdots$ sequence of planes.

within periodically stacked domains which form the partially ordered state taking place below the melt. Therefore the resulting deformation and growth stacking faults preexist in the hcp structures independently from the martensitic transformation between the two structures. When going from one structure to the other domains are created originating in the loss of symmetry operations related to the absence of group-subgroup relationship between the symmetries of the structures.

At the fcc→hcp transformation four types of orientational domains are produced which can be deduced from one another by fourfold cubic rotations or equivalently by the four {111} cubic planes. In the hcp structures two neighboring domains differ by 70.5° as found in Refs. 12 and 13. Figures 7(a) and 7(b) represent two among the cubic domains formed by $BCBCBC\cdots$ sequences of hexagonal close packed planes in the cubic framework and corresponding to hexagonal [0001] direction. In addition each cubic variant gives rise to three types of antiphase domains since the fcc translations are lost in the hcp lattice as shown by Eq. (1), at the corresponding cell doubling transition. Three antiphase domains corresponding to $ABAB\cdots$,$ACAC\cdots$, and $CBCB\cdots$ sequences are represented in Figs. 7(c)–7(e). The full set of twelve (antiphase and orientational) domains have been observed by Bibring and Sebilleau[13] and Nelson and Altstetter[12] whereas the variants associated to only three cubic directions were reported by Gaunt and Christian[71] and Babkevich *et al.*[72]

The reverse hcp→fcc transformation creates also three types of antiphase domains which shift the atoms along the $\{2\bar{1}\bar{1}0\}_L//\{\bar{1}010\}_h$ and $\{\bar{1}2\bar{1}0\}_L//\{0\bar{1}\bar{1}0\}_h$ directions by $|\mathbf{a}_a|/\sqrt{3}$. Figure 7(f) shows one of such cubic domains corresponding to the sequence of hexagonal planes $ABCABC\cdots$. Two other domains ($BCABCA\cdots$ and $CABCAB\cdots$) can be derived from the corresponding shifts of the $ABCABC\cdots$ structure. Since the cubic phase corresponds to a sheared rhombohedral D_{3d}^5 symmetry two types of orientational domains may be produced which transform into one another by the (001) hexagonal plane. However only one variant is generally observed after the transformation from the hcp phase.[23]

As shown in Sec. II C these different symmetry induced variants should produce temperature independent (growth or deformation) stacking faults at variance with the temperature dependent stacking faults inherently associated with a nonmaximal value of the ordering order parameter. The detailed investigation by Frey and Boysen[24] based on elastic neutron scattering data on single crystal conclude that the hcp and fcc phases of Co are disordered by a smaller amount than reported in previous studies on powder samples,[22,73] i.e., 2.5% for the hcp phase and 0.5% for the fcc phase. The degree of disorder in the hcp phase is essentially due to growth faults and is temperature independent when approaching the transformation being also not affected by ageing the sample across the transformation. In contrast the fcc phase, below and above the transformation is well ordered with no evidence of growth faults. However, the observation[12,71] that a crystal of cobalt cycled through the transformation and remaining below 600° C gives on cooling the same single variant in the hcp phase, is in favor of the existence above the transformation of symmetry induced (deformation) stacking faults.

Summarizing the reordering process between the hcp and fcc cobalt phases, assumed in our model takes place from a less ordered hcp to a more ordered fcc structure. In the two phases in the region surrounding the transformation the observed (small) disorder corresponds to symmetry induced stacking faults which are predominantly of the growth type in the hcp phase and of the deformation type in the fcc phase. The residual random disorder associated with the ordering of the two close packed structures below the melt is negligible.

E. Irreversibility of the latent heat and the intermediate 6-layered structure

One of the striking features of the martensitic transformation of cobalt is the fact that the transformation enthalpy Δh

is greater on heating ($\Delta h^h \simeq 113$ cal mol^{-1}) than on cooling ($\Delta h^c = 84$ cal mol^{-1}). This was first reported by Adams and Altstetter[65] and confirmed by Munier *et al.*[74] who found a difference $\Delta h^h - \Delta h^c \simeq 5$ cal mol^{-1}. Both studies also show that when the number of transformation cycles increases Δh diminishes and the hysteresis width increases.[65,74] A similar interpretation of this ''irreversible'' behavior is proposed by the two groups of searchers: Cycling through the transformation induces defects in the two close packed structures and the difference found for $\Delta h^h - \Delta h^c$ is due to the amount of energy needed for their formation. The fact that Δh^h is larger that Δh^c is consistent with the property assumed in our description, that the fcc phase is more ordered than the hcp phase: More energy will be required to create defects in the fcc phase when heating from hcp, than in the hcp phase, on cooling from fcc. A great part of these symmetry induced defects remain in the structures and they influence the following cycles. This explains the diminishing of Δh during the successive transformation cycles. Note that there is no contradiction between a decrease of Δh and an increase of the region of coexistence of the phases as observed by Munier *at al.*[74] since Δh expresses, in part, the energy required to create new defects the number of which decreases on cycling due to saturation. On the other hand the extension of the hysteresis region should be related to a pinning of an increasing number of defects which favors the phase coexistence.

From the values found in Refs. 65 and 74 for $\Delta h^h - \Delta h^c \simeq 5-30$ cal mol^{-1} a rough estimate of the number of stacking faults created in one cycle can be given using the amount of energy $E \sim 10^{-4}$ cal mol^{-1} calculated by Hitzenberger *et al.*[75] necessary to create one stacking fault in hcp cobalt close to the transformation. One gets $N \simeq 10^5$ stacking faults per mole corresponding approximately to one stacking fault every hundred hexagonal planes.

The enlargement of the hysteresis region on cycling across the transformation is consistent with the form of the region of coexistence of the hcp and fcc phases shown in the theoretical phase diagram of Fig. 3(a). This region diverges from the *N*-point enlarging between the lines denoted $3-N$ and $4-N$ in the figure. Crossing the preceding lines one goes from the starting martensite to the starting austenite points denoted M_s and A_s in Ref. 74. Further cycling will shift the thermodynamic path towards a larger region of coexistence of the phases. Figure 4 in Ref. 74 shows that the width of the hysteresis region increases from about $A_s - M_s = 20°\mathrm{C}$ to $A_s - M_s = 47°\mathrm{C}$. Therefore in the initial cycles the thermodynamic path is closer to the three-phase *N* point at which the six-layered phase III begins to be stable and should cross the region comprised between the *MA* line and line 3 in Fig. 3(a). The *MA* line represents the limit of stability of phase III with respect to the fcc phase and line 3, close to the *N* point is the limit of stability of the fcc and six-layered phase within the hcp phase. Hence the preceding region should correspond to the modulated structure of about 20°C extension observed by Blaschko *et al.*[23] This is consistent with the description given by these authors in terms of periodic modulation with a six-layer wavelength of the (111) fcc lattice planes fraction in which platelike nuclei of the hcp phase are coherently inserted into the fcc matrix. In our interpretation the modulated structure reflects the closeness to a stable six-layered phase. An estimate of the location and range of stability of this phase in the pressure-temperature phase diagram of cobalt[76] would require knowledge of the limit of stability lines denoted $3-N$ and $4-N$ in Fig. 3, which have not been determined experimentally in pure cobalt.

It has to be noted that the modulated structure reported by Blaschko *et al.*[23] and confirmed by Babkevitch *et al.*,[72] is not symmetric with respect to the fcc and hcp structures but corresponds to a deformation of the fcc structure since the satellite spots are found about the (111) fcc reflections. Note also that our proposed interpretation is compatible with a description in terms of strain field modulation due to coherency stresses as suggested in Ref. 23, although the coherency stresses should be due to the coexistence of *three* phases (hcp fcc and 6-layered). By contrast it differs from the interpretation given by Babkevitch *et al.*[72] in terms of a nonrandom segregation of impurity atoms occupying part of the layers, or with that of Mishin and Razumovskii[77] who describe the modulation as a pretranslational effect induced by heterophase fluctuations.

F. The phonon spectrum of cobalt and the elastic anomaly

Investigations of the dynamical properties of cobalt[17–21] have been performed in order to verify the eventual existence of a soft-mode in connection with the martensitic nature of the transformation and with the suggestion[78] that its mechanism could be triggered by a small decrease of phonon energy related to small displacements. No softening behavior has been found when approaching the transition either from the hcp (Ref. 19) or fcc (Ref. 17,21) sides. This is consistent with the purely reordering character of the transformation assumed in our approach since the average atomic positions remain fixed across ordering-type transitions and the jumps of atoms between the sites are supposed to be uncorrelated. This picture is still reinforced by the reconstructive character of the transition which as shown in Ref. 64, implies no critical fluctuations.

The absence of temperature dependence of the relevant phonon branches constitutes, however, only a partial confirmation of our proposed reordering type mechanism. A more precise confirmation of the mechanism can be found in the frequency dependence $\omega(\mathbf{k})$ on the reduced $\mathbf{k}$-vector of the phonon spectra as it can be used to verify the coincidence of the structures surrounding the transformation in the directions of space preserved by the reconstruction of the lattice, i.e., one expects to find a coincidence of the phonon branches for the two structures in these directions and a softening of $\omega(\mathbf{k})$ at special points corresponding to the translational connection of the two structures. Let us show that an indirect confirmation of the underlying existence of a latent polytypic phase can be found in the phonon spectra reported for cubic[17,18,21] and hexagonal[19,20] cobalt.

In order to disclose the structural relationship between the fcc and hcp structures in reciprocal space let us represent the

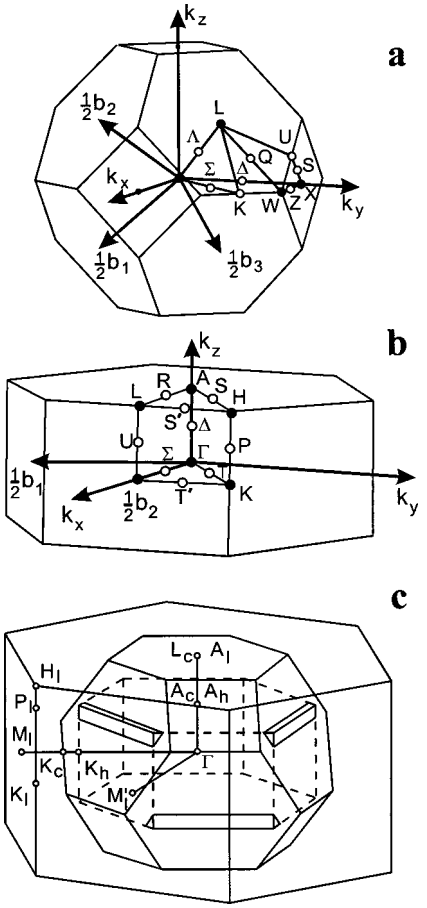

FIG. 8. (a) fcc Brillouin zone. (b) hcp Brillouin zone. (c) Embedding of the fcc and hcp Brillouin zones in the *L*-phase Brillouin zone.

connections between the Brillouin-zones of the three fcc, hcp and *L* structures. Figures 8(a), 8(b), and 8(c) show, respectively, the fcc and hcp Brillouin zones and their embedding within the *L*-hexagonal Brillouin zone. Figure 8(c) reveals that the coinciding symmetry directions for the three zones are $\Gamma A_L = \Gamma L_c = 2\Gamma A_h$ and $\Gamma M_L // \Gamma K_h // \Gamma K_c$ where the indices *L*, *c*, and *h* refer to the *L*, fcc and hcp structures. Figures 9(a) and 9(b) show the phonon spectra obtained for the hcp and fcc phases of Co in the preceding directions. Figure 9(c) represents the superposition of the two spectra the full circles corresponding to hexagonal cobalt[20] and the open circles to cubic cobalt.[17,18] We can verify the following: (i) In the direction ΓA_L there is a perfect coincidence for the full and open circles which lie on the same phonon branches in agreement with the doubling of the basic translation in this direction. (ii) Along the ΓKM reciprocal space direction there is a good agreement for two phonon branches, whereas for the third branch the two structures give different curves. This discrepancy can be explained by the fact that the experiments on fcc and hcp cobalt were performed at temperatures differing by about 700 K,[17,18,20] and by the observation by Frey *et al.*[19] that the slope of this branch increases when the temperature decreases. This explanation is supported by the convergence of the two curves when approaching the transition temperature T_m. Note also that the hexagonal spectrum[20]

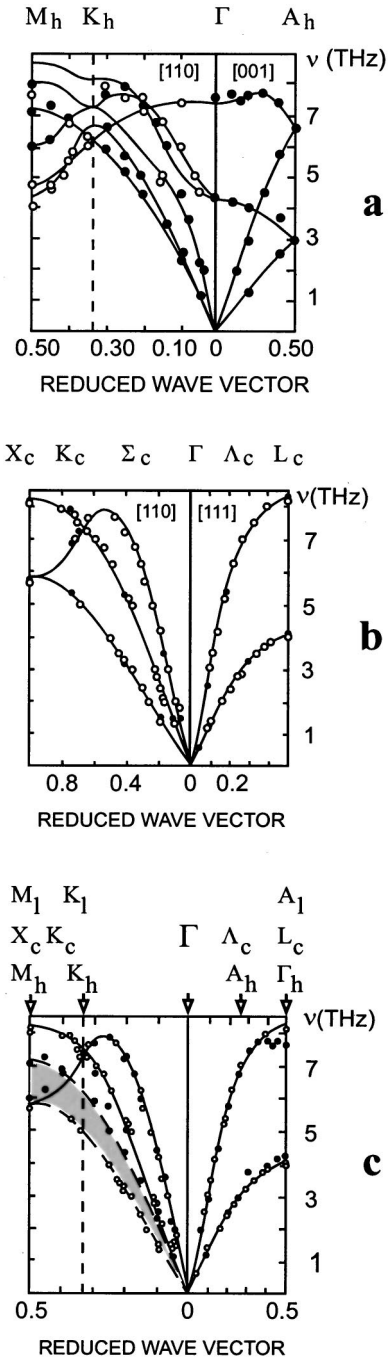

FIG. 9. (a) Phonon spectrum of hexagonal cobalt from Ref. 20. (b) Phonon spectrum of cubic cobalt from Refs. 17,18. (c) Superposition of the two preceding spectra. In (c) full and open circles correspond to hexagonal and cubic cobalt, respectively.

was obtained on pure cobalt while the cubic spectrum was measured on $Co_{0.92}Fe_{0.08}$.[17,18] (iii) The crossing of two branches at the K_h point in the hexagonal spectrum [Fig. 9(a)] is related to the fact that at this point two small IRs of the C_{2v} point group degenerate in a two-dimensional IR of the point group D_{3h}. However the crossing at K_h of the two branches in the cubic spectrum [Fig. 9(b)] despite the fact that this point is not at the surface of the fcc Brillouin zone constitutes a verification of the existence of the *L* structure

since K_h coincides [Fig. 9(c)] with the surface point K_L of the L structure: At K_h the cubic structure is reminiscent of the ''parent'' disordered L structure.

The phonon spectrum may also serve as a test to check the influence of macroscopic deformations which are involved at reconstructive transformation mechanisms as such deformations modify the distance between equivalent sites in the initial and final structure (i.e., they change the *metric* of the structures). The optical phonon curves will thus display shifts with respect to their location in the undeformed structure whereas acoustic phonon branches undergo changes in their slopes. In this respect the small dip of the optical branch reported by Frey *et al.*[19] in the hexagonal phase in the direction ΓA_h at $\frac{2}{3}(0,0,\pi/c)$ on approaching T_m, can be related to the coupling of the primary optical instability to the secondary shear strain e_4 which as noted in Sec. II A is required for the formation of the fcc structure. One has effectively $\frac{2}{3}c_h^*=\frac{1}{3}c_L^*$ which corresponds to the wave vector $\mathbf{k}_{10}$ associated with the $L\rightarrow$fcc virtual transition.

The preceding anomalous dip observed in the hcp phase represents a precursor indication of the shear strain $e_4=e_{yz}$ arising spontaneously in the fcc structure. The corresponding acoustic instability will consist in a decrease in the slope of the hexagonal elastic constant c_{44}. c_{44} actually diminishes about 50 K below T_m from the value 0.7×10^{12} to 0.53×10^{12} dyn/cm^3 at T_m, i.e., $\Delta c_{44}/c_{44}\simeq 27\%$. This has been first observed by Frey *et al.*[19] and confirmed by Strauss *et al.*[21] The elastic constant anomaly is consistent with a dip of the Debye-Waller factor measured by Bokshtein *et al.*[79] and with the increase of the internal friction related by Bidaux *et al.*[68] to shear modes parallel to the hexagonal planes. The fact that in our approach no spontaneous strain is needed as a secondary order-parameter for the formation of the hcp phase is confirmed by the absence of elastic constant anomalies within the fcc phase on approaching T_m and especially of $c'\sim c_{11}-c_{12}+c_{44}$.

G. The high-pressure double hcp phase

Yoo *et al.*[7] disclosed a high pressure phase in Co identified as a double hcp (dhcp) structure. The phase denoted ε', is stabilized on quenching fcc-Co below 60 GPa but not on heating hcp-Co. As the region of stability of the ε' phase lies between the fcc and hcp phases it suggests an adaptive nature for the corresponding structure. The fact that the fcc structure is more ordered than the hcp structure explains why an adaptive structure is required to go through the fcc$\rightarrow$hcp thermodynamic path, i.e., the more defective hcp structure can adapt more easily for a direct hcp$\rightarrow$fcc path. The x-ray patterns reported for $\varepsilon'-$Co (Figs. 1 and 2 in Ref. 7) show that the main Bragg reflections associated with the assumed dhcp structure are surrounded by weak reflections corresponding to a more complex stacking. Such reflections can be interpreted by the property of the four-layered lamellas characterizing a dhcp structure to be surrounded by longer-period polytypes. Note that symmetry considerations (see Secs. II and III E) favor six-layered (thcp) ''adaptive'' lamellas between the hcp and fcc structures. This possibility has not been tested in the structural analysis of the ε' phase.[7]

The ε' phase appears below the extrapolation of the paramagnetic-ferromagnetic transition line within fcc-Co. It indicates that the lowering of energy barrier between the fcc and hcp structures is favored by the onset of the magnetic ordering. Such property can be foreseen by considering the mixed free-energy expansion

$$F'(TP,\varsigma,\eta,M)=F(T,P,\varsigma,\eta)+\frac{d_1}{2}M^2+\frac{d_2}{4}M^4+\frac{\delta_1}{2}M^2\eta^2+\frac{\delta_2}{2}M^2\varsigma^2, \tag{22}$$

where $F(T,P,\varsigma,\eta)$ is the effective order-parameter expansion, given by Eq. (6) associated with the fcc-hcp transformation. The remaining terms in Eq. (22) express the free-energy associated with the onset of the magnetization **M** at the paramagnetic-ferromagnetic transition in fcc Co and the coupling of **M** with the structural order parameter. Minimization with respect to M of F' provides the equation of state

$$M(d_1+d_2M^2+\delta_1\eta^2+\delta_2\varsigma^2)=0 \tag{23}$$

which yields the equilibrium value of M in the ferromagnetic state

$$(M^e)^2=-\frac{1}{d_2}(d_1+\delta_1\eta^2+\delta_2\varsigma^2). \tag{24}$$

Introducing M^e in Eq. (22) gives the renormalized form of F' at lower order

$$F'(T,P,\varsigma,\eta)=F(T,P,\varsigma,\eta)-\frac{d_1^2}{4d_2}-\frac{d_1}{d_2}(\delta_1\eta^2+\delta_2\varsigma^2)+\ldots \tag{25}$$

showing that for $d_2>0$ and $d_1<0$ an attractive coupling ($\delta_1<0\,\delta_2<0$) decreases the value of F and therefore leads[80] to a reduction of the energy barrier between the fcc and hcp phases.

H. The transformation mechanisms between the fcc and hcp structures in cobalt

Let us show that the order-parameter symmetries assumed in Sec. II A for the ordering mechanisms leading to the fcc and hcp structures allow one to account qualitatively for the observations reported for the fcc$\rightarrow$hcp and hcp$\rightarrow$fcc transformations in the series of studies by Karnthaler and his co-workers[53,75,81–84] on cobalt and Co-Ni alloys as well as for the previously proposed mechanisms.[27–35] In Sec. II A, it has been shown that the fcc structure results from specific crystallogeometrical conditions fulfilled by the three-layered rhombohedral structure of symmetry $D_{3d}^5(R\bar{3}m)$ induced in the ordering process, which leads to an enlargement of the rhombohedral symmetry to cubic. Therefore the fcc$\rightarrow$hcp and hcp$\rightarrow$fcc transformations proceed via an underlying intermediate structure.

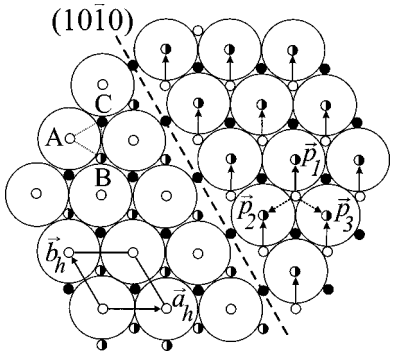

FIG. 10. Onset of a partial in a close packed atomic plane. Small open circles represent positions *A* small full circles are positions *C*. Half-filled small circles are positions *B*. The dashed line represents a glissile Schockley partial dislocation characterized by the $\mathbf{p}_i$ Burgers vector and belonging to the $(10\bar{1}0)$ hexagonal plane.

As already noted in Sec. II A the $O_h^5 \rightarrow D_{3d}^5$ symmetry change corresponds to a ''pseudo-proper'' ferroelastic transition[85] at which the spontaneous strain $e_4 = e_{yz}$ couples bilineary to the primary ordering parameter ς. The shear stress σ_{yz} conjugated to e_{yz} is parallel to the close-packed layers and induces as a secondary effect a deformation coinciding with the strain component e_{xx} between two hexagonal planes where the atoms are, for example in *A* and *C* positions. Such deformation results in a stretching of, let say the *A* atoms, which due to the geometrical constraints, produces a jumplike shifting of the atoms from their *A* positions to the *B* positions as represented in Fig. 10. In this figure one can see that this shifting give rise to the onset of a glissile Schockley partial dislocation (so called ''partial'') characterized by one among the three equivalent Burgers vectors $\mathbf{p}_i$ of the $(\mathbf{a}_h/3)\langle 1\bar{1}00\rangle$ type where $\mathbf{a}_h$ is the hexagonal lattice vector. Note that the onset of a partial in a layer formed by *A* atoms does not deform the layer with atoms in *C* positions, since the *A* atoms are located in the hollows of the *C* layer. Only the atoms of *C* type located above and below the dislocation line can be slightly shifted (but not necessarily) in the [111] cubic direction. The row of these out-of-plane atoms therefore appears as a nucleus for a dislocation in the *C* layer. This process being repeated leads to the growth of an hexagonal lamella in the cubic structure. Besides the set of partials in successive planes appear as a sharp interphase front parallel to the $(10\bar{1}0)$ hexagonal plane [i.e., the cubic (210) plane] (Fig. 10).

The preceding atomistic mechanism is consistent with the dislocation mechanisms assumed in most models of the fcc-hcp transformation.[27–35] and with the direct electron-microscopy observations.[83] An almost similar mechanism leading to the onset of a partial dislocation in a close-packed hexagonal plane may be invoked for the reversed hcp→fcc transformation although it is less directly grounded on the corresponding order-parameter symmetry. The $D_{6h}^4 \rightarrow D_{3d}^5$ symmetry change is an ''improper'' ferroelastic transition,[86] i.e., it corresponds to the spontaneous onset of the elastic constant $c_{14} = c_{xxyz}$ as the result of an improper coupling of the order parameter with c_{14} of the form $\eta^2 c_{14}$. Since the physical quantity conjugated to c_{14} is the stress product $\sigma_{xx}\sigma_{yz}$ it may lead again to the coupled strains e_{xx} and e_{yz} which produce the stretching of hexagonal layers and the resulting partial dislocation shown in Fig. 10. Hence the atomistic mechanism leading to partial dislocations in the hexagonal layers can be only considered as a secondary effect for the hcp→fcc thermodynamic path. A more consistent formation of the hcp→fcc transformation mechanism should be made in terms of an accumulation of stacking faults nucleating initial fcc lamellas of a few atoms in the hcp phase which then grow and expand to form the fcc structure. Such mechanism is supported by the faulting disorder found in the hcp structure (Sec. III D) which is essentially symmetry induced (antiphase domains) as discussed in Sec. II, and does not correspond to a random distribution of stacking faults as assumed by Fujita and Veda[31] or Pandey and Lele.[35] Note, however, that a small amount of disorder in the stacking fault distribution is predicted in our approach due to the nonmaximal character of the ordering parameter Δ expressed by Eq. (10).

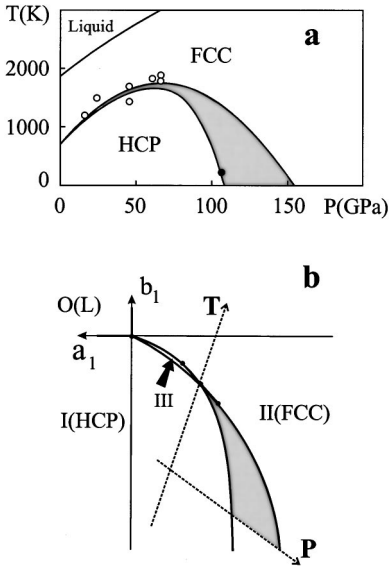

FIG. 11. (a) Experimental phase diagram of cobalt from Refs. 7,87. The shadowed area corresponds to the region of coexistence between the hcp and fcc phases. (b) Theoretical phase diagram in the $(a_1 b_1)$ plane, associated with the free-energy expansion defined by Eq. (26). The dotted arrows represent the pressure and temperature axes in reference to the phase diagram of Fig. 11(a).

I. Comparison with the experimental phase diagram of cobalt

Recently two studies have focused on the experimental phase diagram of cobalt[7,87] which is schematized in Fig. 11(a). One can see that the hcp phase is embedded within the region of stability of fcc cobalt. When comparing with the theoretical phase diagrams of Fig. 3 it clearly appears that the fourth-degree expansion given by Eq. (6) is insufficient to account for the experimental features. Figure 11(b) shows

one of the theoretical phase diagrams associated with the sixth degree expansion in η:

$$F(TP,\zeta,\eta)=F_0(T,P)+a_1\zeta^2+a_2\zeta^3+a_3\zeta^4+b_1\eta^2+b_2\eta^4 + b_3\eta^6+c\zeta^2\eta^2 \quad (26)$$

which differs from the theoretical phase diagram of Fig. 3 by the experimental property that the limit of stability line between the hcp and fcc phases is curved toward the hcp phase as suggested by experimental phase diagram. In order to obtain a suitable fitting with the experimental curves one needs to take into account a linear dependence of three coefficients (a_1,a_2, and b_1) on temperature and pressure. The phase diagram shown in Fig. 11(b) assumes $b_3>0$ and $\Delta_1=b_2^2-3b_1b_3>0$. A more precise quantitative model (with determined numerical values of the coefficients) would require more experimental points for the phase boundaries.

V. SUMMARY AND CONCLUSION

The present work deals with a general phenomenological description of the transformation between the fcc and hcp structures which is applied to the illustrative example of cobalt. The following results are independent from the specific situation found in cobalt.

(1) The fcc and hcp structures can be described as resulting from different ordering mechanisms from a disordered polytypic structure. Within the segregation process leading to the formation of close-packed structures from the melt the fcc and hcp structures are assumed to order progressively via a periodic array of stacked domains in which lamellas of the ordered structures are surrounded by disordered sequences of hexagonal layers. On approaching the fully ordered states the fraction of disordered polytype sequences reduces in each domain increasing the thickness of the lamellas, and simultaneously the neighboring domains coalesce. The direct reconstructive reordering mechanism between the fcc and hcp structure involves an underlying rhombohedral intermediate structure which produces in both the fcc→hcp and hcp →fcc thermodynamic paths a shear strain e_{yz} giving rise to glissile partial dislocations acting as nuclei for the formation of hcp and fcc lamellas. Note that these pretransitional lamellas are different in origin and nature from the lamellas invoked in the segregation process of the close packed structures.

(2) The preceding picture of the fcc-hcp transformation has to be completed by the property of the two structures to be intrinsically faulted due to symmetry induced antiphase and orientational domains. There are also temperature dependent stacking faults which originate in the nonmaximal character of the order-parameter inherent to the assumed ordering mechanism.

(3) Other general properties of the fcc-hcp transformation which result from the reconstructive and ordering characters of this transformation are (i) the absence of soft mode behavior which does not exclude the softening of elastic constants related to secondary strains. (ii) The typical δ-shaped anomaly of the specific heat. (iii) The existence of a six-layered structure intermediate between the fcc and hcp structures which is stabilized in a region of the phase diagram close to the disordered polytype regime.

A number of general symmetry arguments have been given for explaining the asymmetric features characterizing the transformation in cobalt such as, for example, (i) the asymmetry of the interphase region which has been related to the property of the fcc and hcp structures to correspond to distinct subgroup symmetries of the parent disordered phase and (ii) the difference in the fcc→hcp and hcp→fcc mechanisms which have been deduced from the different strains and couplings involved by the underlying rhombohedral structure. However, the asymmetry of the thermodynamic fcc→hcp paths seems to be more enhanced in cobalt due to the specific property of the fcc and hcp structures in this element to display a different degree of order. This property results, for example, in different transformation enthalpies for the two paths which is not a general feature of the fcc-hcp transformation.

In a recent study devoted to the phase transformations in lithium and sodium[80] the properties characterizing reconstructive martensitic transformations of the displacive type were underlined. From the present study one can verify that reconstructive martensitic transformations induced by a reordering mechanism present drastically different theoretical features, namely, (1) the parent phase (e.g., the bcc phase in Li and Na) is adjacent to the transformation in the displacive case whereas the parent polytypic structure does not in general, correspond to a definite region of the phase diagram for reordering martensitic transformations. (2) Although secondary spontaneous strains are required in both types of transformations they play an essential role in the symmetry breaking mechanism leading to displacive martensites whereas they only take part to the transformation kinetics in the reordering mechanism. (3) The precursor effects show important differences. A slight softening of the phonon mode associated with the order parameter can be observed on approaching displacive martensitic transformations while no softening occurs for reordering type martensitic transformations. Conversely a nucleation process is hardly evidenced in the displacive case while it is clearly observed (lamellas) in the reordering mechanism. There is however, an essential common theoretical property of the phases surrounding displacive or reordering martensitic transformations of the reconstructive type. In both cases the phases coincide with limit states which result either from fixed critical displacements (and fixed critical strains) or from definite crystallogeometrical conditions, required for the formation of close packed structures.

ACKNOWLEDGMENTS

We are grateful to Dr. T. Waitz and Professor H. P. Karnthaler for helpful discussions on the mechanism of the fcc-hcp and hcp-fcc transformations, to S. B. Rochal for allowing reproduction of Fig. 3 and to the Swiss National Science Foundation for financial support. The work was partly supported by the Fonds zur Forderung der wissenschaftlichen Forschung in Austria.

APPENDIX

Generators of the 2×2 matrices forming the IR $\tau_1(\mathbf{k}^*_{15})$ associated with the $D^1_{6h}\rightarrow D^4_{6h}(V\times6)$ $(L\rightarrow\text{hcp})$ transition

$$\{C_6|000\}\{I|000\} \quad \{C_1|3\mathbf{c}_L\} \quad \{C_1|\mathbf{a}_L\} \quad \{C_1|4\mathbf{a}_L\}$$
$$\begin{bmatrix}0&1\\1&0\end{bmatrix} \quad \begin{bmatrix}-1&0\\0&-1\end{bmatrix} \quad \begin{bmatrix}\varepsilon&0\\0&\varepsilon^*\end{bmatrix} \quad \begin{bmatrix}1&0\\0&1\end{bmatrix}.$$

Generators of the 4×4 matrices forming the IR $\tau_1(\mathbf{k}^*_{10})$ associated with the $D^1_{6h}\rightarrow D^5_{3d}(V\times3)$ $(L\rightarrow\text{fcc})$ transition

$$\{C_6|000\} \quad \{I|000\} \quad \{C_1|3\mathbf{c}_L\}$$
$$\begin{bmatrix}0&0&0&1\\0&0&1&0\\0&1&0&0\\1&0&0&0\end{bmatrix} \quad \begin{bmatrix}0&1&0&0\\1&0&0&0\\0&0&0&1\\0&0&1&0\end{bmatrix} \quad \begin{bmatrix}1&0&0&0\\0&1&0&0\\0&0&1&0\\0&0&0&1\end{bmatrix},$$

$$\{C_1|\mathbf{a}_L\} \quad \{C_1|4\mathbf{a}_L\}$$
$$\begin{bmatrix}\varepsilon&0&0&0\\0&\varepsilon^*&0&0\\0&0&\varepsilon&0\\0&0&0&\varepsilon^*\end{bmatrix} \quad \begin{bmatrix}\varepsilon&0&0&0\\0&\varepsilon^*&0&0\\0&0&\varepsilon^*&0\\0&0&0&\varepsilon\end{bmatrix}.$$

[1] D.A. Young, *Phase Diagrams of the Elements* (University of California Press, Berkeley, 1991).
[2] Lin-Gun Liu and W.A. Bassett, *Elements, Oxides and Silicates* (Oxford University Press, Oxford, 1986).
[3] E.G. Bain, Trans. AIME **70**, 25 (1924).
[4] W.G. Burgers, Physica (Amsterdam) **1**, 561 (1934).
[5] V.P. Dmitriev, S.B. Rochal, Yu.M. Gufan, and P. Tolédano, Phys. Rev. Lett. **60**, 1958 (1988).
[6] V.P. Dmitriev, Yu.M. Gufan, and P. Tolédano, Phys. Rev. B **44**, 7248 (1991).
[7] C.S. Yoo, P. Söderlind, and H. Cynn, J. Phys.: Condens. Matter **10**, L311 (1998).
[8] C.A. Vanderborgh, Y.K. Vohra, H. Xia, and A.L. Ruoff, Phys. Rev. B **41**, 7338 (1990).
[9] C.S. Barrett and T.B. Massalski, *Structure of Metals* (McGraw Hill, New York, 1966).
[10] Z. Nishiyama, *Martensitic Transformations* (Academic Press, New York, 1978).
[11] A.R. Troiano and J.L. Tokich, Trans. Am. Inst. Min., Metall. Pet. Eng. **175**, 728 (1948).
[12] J.O. Nelson and C.J. Altstetter, Trans. AIME **230**, 1577 (1964).
[13] H. Bibring and F. Sebilleau, Rev. Met. **52**, 569 (1955).
[14] T. Onozuka, S. Yamaguchi, M. Hirabayashi, and T. Wakiyama, J. Phys. Soc. Jpn. **37**, 687 (1974).
[15] B.I. Nikolin, A.Yu. Babkevich, T.L. Sizova, and N.N. Shevchenko, Scr. Metall. **22**, 761 (1988).
[16] *Handbook of Thermophysical Properties of Solid Materials. I. Elements* (Pergamon Press, Oxford, 1961) p. 142.
[17] S.M. Shapiro and S. Moss, Phys. Rev. B **15**, 2726 (1977).
[18] E.C. Svensson, B.M. Powell, D.B. Woods, and W. Teuchert, Can. J. Phys. **57**, 253 (1979).
[19] F. Frey, W. Prandl, J. Schneider, C. Zeyen, and K. Ziebeck, J. Phys. F: Met. Phys. **9**, 603 (1979).
[20] N. Wakabayashi, R.H. Schermand, and H.G. Smith, Phys. Rev. B **25**, 5122 (1982).
[21] B. Strauss F. Frey, W. Petry, J. Trampenau, K. Nikolaus, S.M. Shapiro, and J. Bossy, Phys. Rev. B **54**, 6035 (1996).
[22] O.S. Edwards and H. Lipson, Proc. R. Soc. London, Ser. A **180**, 268 (1942).
[23] O. Blaschko G. Krexner, J. Pleschiutschnig, G. Ernst, C. Hitzenberger, H.P. Karnthaler, and A. Korner, Phys. Rev. Lett. **60**, 2800 (1988).
[24] F. Frey and H. Boysen, Acta Crystallogr., Sect. A: Cryst. Phys., Diffr., Theor. Gen. Crystallogr. **37**, 819 (1981).
[25] B.I. Nikolin, A.Yu. Babkevich, T.V. Izdkovskaya, and S.N. Petrova, Acta Metall. Mater. **41**, 513 (1993).
[26] S.A. Demin, A.A. Nekrasov, and A.I. Ustinov, Acta Metall. Mater. **41**, 2091 (1993).
[27] J.W. Christian, Proc. R. Soc. London, Ser. A **206**, 61 (1951).
[28] Z.S. Basinski and J.W. Christian, Philos. Mag. **44**, 791 (1953).
[29] A. Seeger, Z. Metallkd. **44**, 247 (1953); **47**, 653 (1956).
[30] W. Bollmann, Acta Metall. **9**, 972 (1961).
[31] H. Fujita and S. Veda, Acta Metall. **20**, 759 (1972).
[32] G.B. Olson and M. Cohen, Metall. Trans. A **7**, 1897 (1976).
[33] S. Mahajan, M.L. Green, and D. Brasen, Metall. Trans. A **8**, 283 (1977).
[34] J. Singh and S. Ranganathan, Phys. Status Solidi A **73**, 243 (1981).
[35] D. Pandey and S. Lele, Acta Metall. **34**, 415 (1986).
[36] I. Folkins and M.B. Walker, Phys. Rev. Lett. **65**, 127 (1990).
[37] R. Bruinsma and Z. Zangwill, Phys. Rev. Lett. **55**, 214 (1985).
[38] R. Bruinsma and Z. Zangwill, Comments Condens. Matter Phys. **13**, 1 (1987).
[39] R. Bruinsma, Phase Transitions **16-17**, 275 (1989).
[40] V.P. Dmitriev S.B. Rochal, Yu.M. Gufan, and P. Tolédano, Phys. Rev. Lett. **62**, 2495 (1989).
[41] A.R. Verma and P. Krishna, *Ploymorphism and Polytypism in Crystals* (Wiley, New York, 1966).
[42] N.V. Belov, *Structure of Inorganic Crystals and Metallic Phases* (AN SSSR Publications, Moscow, 1947).
[43] O.V. Kovalev, *Irreducible Representations of the Space Groups* (Gordon and Breach, New York, 1965).
[44] J. Zak, A. Casher, H. Glück, and Y. Gur, *The Irreducible Representations of Space Groups* (Benjamin, New York, 1969).
[45] J.-C. Tolédano and P. Tolédano, *The Landau Theory of Phase Transitions* (Word Scientific, Singapore, 1987).
[46] S. B. Rochal, candidate dissertation, University of Rostov on the Don, 1989.
[47] H. Jagodinski, Acta Crystallogr. **7**, 300 (1954).
[48] V. Dmitriev P. Tolédano, A.M. Figueiredo Neto, and I.V. Leb-

edyuk, Phys. Rev. E **59**, 771 (1999).
[49] Wu-Ki Tung, *Group Theory in Physics* (World Scientific, Singapore, 1985).
[50] L. Michel, Rev. Mod. Phys. **52**, 617 (1980).
[51] This result is general for order-disorder transitions in crystals when the parent phase unit cell has only onefold position occupied.
[52] Such description assumes that below the melt preformed hexagonal layers are the subunits and not the atoms. It is analogous to the description of lamellar states in lyotropic complex fluids (Ref. 48).
[53] T. Wartz and H.P. Karnthaler, Philos. Mag. A **73**, 365 (1996), and references therein.
[54] H.T. Davis, *Introduction to Nonlinear Differential and Integral Equations* (Dover, New York, 1962), p. 209.
[55] The general solution is of the form $\int[a_1y^2+a_2y^3+a_3y^4+c_1]dy=z+c_2$ where c_1 and c_2 are constants.
[56] M.H. Vaynberg and V.A. Trenogin, *Theory of Branching of Solutions of Nonlinear Equations* (Noordhoff Publishing, Leyden, 1974).
[57] R. Hultgren P.R. Desai, D.T. Hawkins, M. Gleiser, K.K. Kelley, and D.D. Wagman, *Selected Values of the Thermodynamic Properties of the Elements* (American Society for Metals, Metals Park, Ohio, 1973), p. 278.
[58] N.A. Nikolaev and L.G. Khvostantsev, Sov. Phys. JETP **65**, 205 (1987).
[59] N.A. Nikolaev, L.G. Khvostantsev, V.E. Zinoviev, and A.A. Sirotin, Sov. Phys. JETP **64**, 589 (1986).
[60] J.P. Frank, Phys. Rev. B **22**, 4315 (1980).
[61] J.P. Frank and W.B. Daniels, Phys. Rev. Lett. **44**, 259 (1980).
[62] B.I. Min, T. Oguchi, and A.J. Freeman, Phys. Rev. B **33**, 7852 (1986).
[63] P. Söderlind, R. Ahuja, O. Eriksson, J.M. Wills, and B. Johansson, Phys. Rev. B **50**, 5918 (1994).
[64] P. Tolédano and V. Dmitriev, *Reconstructive Phase Transitions in Crystals and Quasicrystals* (World Scientific, Singapore, 1996).
[65] R. Adams and C. Altstetter, Trans. AIME **242**, 139 (1968).
[66] J. Donohue, *The Structure of the Elements* (Wiley, New York, 1974).
[67] Ref. 16, p. 233.
[68] J.E. Bidaux, R. Schaller, and W. Benoit, Acta. Metall. **37**, 803 (1989).
[69] V.P. Dmitriev, P. Tolédano, V.I. Torgashev, and E.K.H. Salje, Phys. Rev. B **58**, 11911 (1998).
[70] $S(T)$ has a steplike behavior as the order parameter, which can be described by a Heavyside distribution, the derivative of which is a δ function.
[71] P. Gaunt and J.W. Christian, Acta Metall. **7**, 529 (1959).
[72] A.Yu. Babkevich, F. Frey, and H. Kahlert, Philos. Mag. A **72**, 1341 (1995).
[73] S. Kajiwara, Jpn. J. Appl. Phys. **9**, 385 (1970).
[74] A. Munier, J.E. Bidaux, R. Schaller, and C. Esnouf, J. Mater. Res. **5**, 769 (1990).
[75] C. Hitzenberger, H.P. Karnthaler, and A. Korner, Acta Metall. **33**, 1293 (1985).
[76] A quantitative model using the free-energy given by Eq. (6) could predict the location in the pressure-temperature phase diagram of a six-layered phase in ^{4}He [V.P. Dmitriev and S.B. Rochal, J. Low Temp. Phys. **14**, 456 (1988)] and Pr (Refs. 46,64).
[77] Yu.M. Mishin, and I.M. Razumovskii, Acta Metall. Mater. **40**, 2707 (1992).
[78] J.A. Krumhansl and R.J. Gooding, Phys. Rev. B **39**, 3047 (1989).
[79] B.S. Bokshtein, Yu.B. Voitkovskii, G.S. Nikol'skii, and I.M. Razumovskii, Sov. Phys. JETP **37**, 283 (1973).
[80] O. Blaschko, V. Dmitriev, G. Krexner, and P. Tolédano, Phys. Rev. B **59**, 9095 (1999).
[81] C. Hitzenberger, H. Karnthaler, and A. Korner, Acta Metall. **36**, 2719 (1988).
[82] C. Hitzenberger and H.P. Karnthaler, Philos. Mag. A **64**, 151 (1991).
[83] T. Waitz and H.P. Karnthaler, Acta Metall. **45**, 837 (1997).
[84] T. Waitz and H.P. Karnthaler, Phase Transitions **67**, 695 (1999).
[85] J.-C. Tolédano and P. Tolédano, Phys. Rev. B **21**, 1139 (1980).
[86] J.-C. Tolédano and P. Tolédano, Phys. Rev. B **16**, 386 (1977).
[87] C.S. Yoo, H. Cynn, P. Soderlind, and V. Iota, Phys. Rev. Lett. **84**, 4132 (2000).